TECHNICAL MEMORANDUM

631

An Initial Evaluation of FY-3A Satellite Data

Qifeng Lu [1], W. Bell, P. Bauer, N. Bormann and C. Peubey

Research Department

[1] National Satellite Meteorological Center / China Meteorological Administration (NSMC/CMA)

July 2010

European Centre for Medium-Range Weather Forecasts
Europäisches Zentrum für mittelfristige Wettervorhersage
Centre européen pour les prévisions météorologiques à moyen terme

Abstract

FY-3A, launched in May 2008, is the first in a series of seven meteorological satellites due to be launched in the period leading up to 2020 by China's Meteorological Administration. The FY-3A payload includes four instruments of particular interest for NWP: microwave temperature and humidity sounders; a microwave imager; and an infrared sounder. During 2009 data from the calibration-validation phase of the FY-3A mission were introduced into the ECMWF Integrated Forecasting System in order to assess data quality and provide feedback to FY-3A instrument teams. An analysis of first guess departures has shown the data to be of good quality overall. Several issues with instrument performance and ground segment processing have been identified. The most serious of these are: uncertainties in the temperature sounder passbands on-orbit; orbital biases in the infrared instrument affecting the highest peaking channels; and scan biases in the microwave humidity sounder. Variational bias correction partially corrects for these errors but more work remains to be done to correct the problems before operational implementation. In observing system experiments the FY-3A instruments, both individually and as a package, show considerable skill when added to *observation depleted* control experiments. When added to a full observing system the impacts are neutral to slightly positive, as expected. These initial results are encouraging and build confidence that the following series of FY-3 instruments will be widely used in NWP data assimilation systems. Preparations are underway to assess data from the next satellite in the series: FY-3B, due to be launched later in 2010.

1   Introduction

Since the start of China's meteorological satellite programme in 1969 two parallel research and development strategies have been followed. The first involves the exploitation of data from existing satellite instruments, launched by other national agencies. The second involves the development and deployment of China's own series of meteorological satellites. China has successfully launched and operated both geostationary and polar orbiting satellites (Li (2001), Meng (2004)) which have been named *FengYun*, meaning *wind cloud*, often shortened to FY-*N*. Odd *N* denote the polar orbiting series, whereas even *N* denote the geostationary series.

Following the launch of China's first polar orbiting satellite (FY-1A) in 1988, China has launched a series of four further polar orbiters (FY-1B/C/D and FY-3A) and five geostationary satellites (FY-2A/B/C/D/E). Both programmes will continue over the next decade and an ambitious schedule of launches in currently planned, accommodating increasingly sophisticated sensors for operational meteorology.

FY-3A is the preparatory platform for the subsequent series of six polar-orbiting satellites (FY-3B - FY-3G) currently planned for launch between 2010 and 2020. FY-3A was launched from the Taiyuan Launching Centre on May 27, 2008. The 18m^3, 2300 kg payload of FY-3A comprises a suite of 11 instruments (Dong et al. (2009), Zhang et al. (2009)). Of particular interest for NWP data assimilation are the three instruments which make up the Vertical Atmospheric Sounder System (VASS): the Microwave Temperature Sounder (MWTS); the Microwave Humidity Sounder (MWHS) and the Infrared Atmospheric Sounder (IRAS). These cross-track scanning instruments are similar, but not identical, in specification to the Microwave Sounding Unit (MSU), the Advanced Microwave Sounding Unit-B (AMSU-B, recently replaced by the US/European Microwave Humidity Sounder, or MHS) and the High Resolution Infrared Sounder (HIRS) carried originally on the US Polar Orbiting Environmental Satellite System (POES) (Goodrum et al. (2009)). Also of interest for NWP is the 10-channel Microwave Radiation Imager (MWRI), a conical scanning instrument similar in specification to the Advanced Microwave Scanning Radiometer (AMSR) (Kawanishi et al. (2003)).

As a preparatory platform it is important that the performance of the FY-3A sensors is assessed carefully, in order that any deficiencies in the design or on-orbit operation of the instruments can be addressed in future instruments. A cooperation agreement between ECMWF and CMA facilitated an opportunity to assess the FY-3A data at ECMWF immediately after the completion of the early on-orbit testing phase. As part of a comprehensive calibration/validation programme radiances measured by the suite of VASS sounders as well as

the MWRI have been compared to radiances modelled from NWP background fields, using radiative transfer modelling. This approach is now common practise as the high accuracy of NWP fields, coupled with accurate radiative transfer calculations permits the detection of systematic errors in the satellite measured radiances (Bell and Coauthors (2008), Bormann (2009)). For example, for temperature sounding radiances modelled brightness temperatures can reveal systematic errors of a few tenths of a Kelvin in measured brightness temperatures. For moisture sounding channels the sensitivity is lower, but errors of around 1K can be detected using this technique.

This report describes an initial evaluation of FY-3A data using the ECMWF Integrated Forecasting System (IFS). This evaluation has focused on assessing data quality through an inspection of first guess departure fields and associated statistics. The data has also been assessed through Observing System Experiments (OSE's) in which data from the four FY-3A instruments have been introduced into baseline (observation depleted) and full-system experiments, in order to assess the impact on NWP analyses and forecasts.

In Section 2 a more complete description of the FY-3A instrument characteristics is given. In Section 3 the assessment of data quality is presented based on an analysis of first guess departures. Observing system experiments are described in Section 4 and some conclusions and suggestions for future work are drawn in Section 5.

2 The FY-3A Satellite and Instruments

2.1 FY-3A

FY-3A is a sun-synchronous polar-orbiting environmental satellite with an orbital inclination of 98.8°. The satellite platform is a hexahedron of dimensions 4.4×2.0×2.0 meters with a total mass of approximately 2300 kg. Attitude control of the satellite is achieved through three-axis stabilisation with a measuring precision of 50 meters from the on-board star sensor. The altitude of FY-3A is 831 km giving an orbital period of 102 minutes (equivalent to 14 orbits per day). The design life of FY-3A is three years.

The FY-3A global data receiving network is made up of four domestic ground stations (Beijing, Guangzhou, Urumqi and Jiamusi), and a high-latitude station at Kiruna. The data received from Kiruna station arrives at Beijing with a delay of about 3.5 hours. FY-3A data can be obtained by users in several ways. Firstly, the FY-3A spacecraft has a direct broadcast system for real-time broadcasting of all FY-3A data. Users worldwide can receive High Resolution Picture Transmission and Mission Picture Transmission (HRPT and MPT) data using their own receiving facilities and process *via* a software package which is currently under development by the National Satellite Meteorological Center of China Meteorological Administration (NSMC/CMA). Secondly, users can obtain data through the FENGYUN-cast system operated by the National Meteorological Information Center of the China Meteorological Administration (NMIC/CMA). A third option uses a web-based system at NSMC (online at *http://fy3.satellite.cma.gov.cn*).

The FY-3A spacecraft carries eleven instruments and in this study we focus on the four instruments of the VASS package of most interest for NWP data assimilation, *i.e.* the MicroWave Temperature Sounder (MWTS), the MicroWave Humidity Sounder (MWTS), the InfraRed Atmospheric Sounder (IRAS) and the MicroWave Radiation Imager (MWRI).

2.2 Microwave Temperature Sounder (MWTS)

Until the recent advent of advanced IR sounding instruments, microwave temperature sounding data from high performance radiometers was the single most important satellite data type in NWP data assimilation systems (English et al. (2004)). Microwave temperature sounding data, by proving accurate information for the analysis of mass fields, is still a key component of NWP data assimilation systems.

The FY-3A Microwave Temperature Sounder is a four channel cross-track scanning radiometer similar in specification to the Microwave Sounding Unit (MSU) carried on NOAA-8-NOAA-14. The channel characteristics are shown in Table 1. The main reflector of the instrument is rotated through a single measurement cycle once every 16 seconds to give, for each scanline, 15 scene fields of view together with a view of cold space and the on-board warm calibration target. The cold space and warm target views are used to perform a two point radiometric calibration, mapping dimensionless scene *counts* to brightness temperatures, every scanline. The swath width is 2250 km.

The reflector aperture is 10.7 cm in diameter which gives rise to a footprint diameter of 62 km at nadir. From Table 1 it can be seen that designed radiometric sensitivity, expressed as a noise equivalent brightness temperature (NEΔT) is approximately 0.4 K for the channels 2-4. This is contrasted in Table 1 with the lower NEΔTs for the AMSU-A equivalent channels. It is expected that the largest impacts on forecast accuracy for the VASS suite will result from the use of the MWTS radiances. Furthermore, it has been shown in recent studies (Bell et al. (2010)) that the impact of microwave sounding data on analysis and forecast accuracy is sensitive to the radiometric noise performance of temperature sounding channels. It is therefore to be expected from the outset that the positive impact of the MWTS instrument will be less than that obtained from AMSU-A, with lower noise levels and a more complete set of temperature sounding channels spanning the troposphere and lower stratosphere.

The specifications of MWTS instruments for subsequent FY-3 missions will be progressively improved. For example FY-3D, which is currently planned for launch in 2014, will carry a 13 channel MWTS instrument.

2.3 Microwave Humidity Sounder (MWHS)

Microwave sounding channels spanning the water vapour absorption line at 183 GHz have been shown to provide important information for the analysis of upper tropospheric humidity in global data assimilation systems (Andersson et al. (2007)). To date this data has been provided by sensors on the NOAA POES platforms (AMSU-B and MHS) and more recently the European MetOp-A platform (MHS).

The MicroWave Atmospheric Humidity Sounder (MWHS) on-board FY-3A is a 5-channel instrument similar in specification to AMSU-B/MHS with channels in the frequency range 150-183 GHz. The channel characteristics are shown in Table 2. MWHS has an aperture of 14 cm, giving a nominal field of view of 15km at nadir. MWHS differs from AMSU-B in that it includes a dual-polarisation channel at 150 GHz (v, h) (channels 1 and 2 respectively) rather than including a channel at 89 GHz. Compared to AMSU-B, MWHS has 98 steps per scanline over the 2700 km swath while AMSU-B has 90 steps per scanline over a 2250 km swath. The radiometric performance of MWHS is very similar to that of AMSU-B/MHS.

It is planned that the MWHS will be further improved for FY-3D through the inclusion of 3-channels in the 118 GHz band. These channels will provide information on temperature, water vapour and cloud fields which complements that available from traditional sounding and imaging channels.

2.4 Infrared Atmospheric Sounder (IRAS)

Infrared sounders have been used for NWP data assimilation since the launch of the first HIRS instrument on NIMBUS 6 in 1975. Originally designed to be the primary temperature sounding instrument on the TOVS/ATOVS platforms, the practical difficulties of reliably screening the IR measurements for cloud radiative effects as well as the reduced coverage due to cloud contamination has reduced the impact of filter based IR radiometric data. Consequently microwave sounders have had a more significant positive impact in NWP DA systems. The introduction of advanced high resolution infrared instruments based on high performance interferometers (IASI Challon et al. (2001)) or grating spectrometers (*eg* AIRS LeMarshall et al. (2006)) offering high spectral resolution, wide spectral coverage, excellent radiometric performance and hence enhanced information in the vertical has elevated the importance of IR sounding data for NWP data assimilation applications. There is evidence that these instruments have the largest impact of any observation type in NWP DA systems (Hilton et al. (2009), Cardinali *pers. comm.*).

As a first step towards an FY-3 advanced IR sounding capability the InfRared Atmospheric Sounder (IRAS), a HIRS/3-like instrument, is the primary sounder for FY-3A. IRAS has a total of 26 channels, the first 20 of which are similar to HIRS/3 channels while the six additional channels enable IRAS to measure aerosols, carbon dioxide columns, and cirrus clouds. The channel specifications of the IRAS instrument are given in Table 3. The instrument is a cross-track scanning radiometer with a ground footprint 17 km in diameter at nadir. Calibration is achieved once every 40 scanlines by a two point calibration based on deep space views and warm target views.

2.5 Microwave Radiation Imager (MWRI)

The MicroWave Radiation Imager (MWRI) is a conical-scanning microwave imager operating at five frequencies in the range 10-89 GHz, each with dual polarisation, giving 10 channels in total. The channel specifications are shown in Table 4. MWRI has an aperture of 90 cm, giving a frequency dependent ground footprint in the range 12-80km over a swath width of 1400 km. This contrasts with SSMI, for example, which has a main reflector 60 cm in diameter, giving ground footprints in the range 12-25 km over a swath of 1400 km.

In common with most conical scanning radiometers calibration is achieved by a two point radiometric calibration using cold space and warm target views observed once per scanline. Integration times of 2.7 msecs per footprint lead to NEΔT values as shown.

The rotation of the main reflector of the FY-3A MWRI has led to imbalances in the FY-3A platform and this has resulted in an observing strategy in which the MWRI is only spun-up and operated for short and intermitent periods. The assessment of the data in the following sections has been based on some of the available data segments, obtained during the period 10-17 September 2008 and 10-20 October 2008.

3 Data Monitoring and Assessment

The capability to process FY-3A data was developed in IFS (building on CY35R2) during 2009. Following the processing schemes for the analogous POES/MetOp-A instruments, IRAS, MWTS and MWHS data was processed using the *clear-sky* stream, whereas the MWRI data was processed using the *all-sky* stream (Bauer et al. (2010), Geer et al. (2010) and Geer and Bauer (2010)). Key technical details of the implementation are summarised in Table 5 for reference. The FY-3A IFS technical changes were implemented in CY36R3 and, subsequently, the capability to process FY-3B data was implemented in CY36R4

3.1 Coverage, Observed Brightness Temperatures and First Guess Departure Fields

FY-3A is in a morning orbit with a local equatorial crossing time (ascending/descending) of 10:05 and 22:05. This is 30 minutes later than MetOp-A and 1 hour later than NOAA-17. Figure 1 shows that there is considerable overlap of the FY-3A MWTS swath with other satellites, nevertheless FY-3A complements the coverage provided by Metop AMSU-A.

MWRI data was only available for descending sections of the orbit which prevented a meaningful comparison with AMSR-E observations, but a comparison of the observed brightness temperatures from the MWTS, MWHS and IRAS instruments with the analogous MetOp-A ATOVS instruments is presented in Sections 3.1.1, 3.1.2 and 3.1.3 respectively below.

3.1.1 Microwave Temperature Sounder (MWTS)

The swath width of 2250 km results in FY-3A MWTS achieving near-global coverage in each 12 hour assimilation window. Figure 2 shows the observed brightness temperature fields for each of the four MWTS channels (1-4). Shown for comparison in Figure 2 is the observed brightness temperatures for the equivalent AMSU-A channels (3, 5, 7 and 9 respectively) from MetOp-A. The observed brightness temperature fields are broadly similar. The smaller number of footprints for the MWTS (15, compared to 30 for AMSU-A) gives rise to an apparent partial *quantisation* of the brightness temperature histograms for MWTS, most evident for MWTS channels 2 and 3. This is to be expected. A feature of more concern is the apparent +2K shift in the peak of the distribution for MWTS channel 4 relative to AMSU-A channel 9. The brightness temperatures at this peak are associated with observations in the tropics. One possible explanation for this effect is that a shift in the passband of the radiometer, relative to the nominal specification, would give rise to a shift in measured brightness temperatures. The magnitude of this bias should be related to the local lapse rate in the tropical lower stratosphere where MWTS channel 9 peaks. Measurements of the passbands from pre-launch testing of the instrument, which became available during this assessment, are shown in Table 6. The pre-launch measurements show shifts of 40 MHz for channel 4 relative to the specified passband. There is also evidence of shifts in the other MWTS channels.

Figure 3 shows the nominal channel passbands for MWTS and for AMSU-A channels 3-10. For the common passbands the band specifications are very similar. As can be seen from Figure 3, the passband for MWTS channel 4 is located in the relatively flat spectral region midway between two adjacent O_2 absorption lines. Any shift in the frequency of the passband will result in the instrument sampling an optically deeper part of the spectrum, resulting in an upwards displacement of the weighting function. For MWTS channel 4, with a weighting function that peaks in the lower stratosphere where temperatures are close to a minimum, this displacement is associated with elevated observed brightness temperatures.

To estimate the magnitude of the channel frequency drift required to produce a 2K shift in observed brightness temperatures some calculations were carried out using a line-by-line radiative transfer model (Matricardi et al. (2006)). Brightness temperatures were computed for an ensemble of atmospheric profiles drawn from a diverse profile dataset (Chevallier et al. (2006)) assuming frequency shifts in the range ± 200 MHz. These are large frequency shifts, and normally it would be expected that on-orbit passbands would drift by less than ± 1.5MHz for these channels, however such large drifts are required to explain errors of 2K. Figure 4 shows the result of these calculations and demonstrates that a shift of +100 MHz, or -100 MHz gives a reasonable fit to the estimated error in the brightness temperatures. The error here is estimated as the difference between FY-3A and AMSU-A brightness temperatures (*ie* AMSU-A is taken here as a proxy for the true brightness temperature). Simulations of the effects of drifts of 160 MHz or 200 MHz give significantly worse fits to the estimated errors. Furthermore the form of the simulated error, showing a primary maximum in the latitude band ± 30° and a

secondary maximum in the southern polar region is in agreement with the estimated errors. The symmetry of the spectrum in the region around the passband makes it very difficult to estimate the sign of the drift.

To further confirm the hypothesis that the error is due to a significant channel frequency drift, and to provide new pass band specifications, it will be necessary to generate new radiative transfer coefficients assuming a frequency drift of around 100 MHz. By an iterative process it should be possible to improve estimates of the on-orbit passband parameters for MWTS. At the current time a study supported by EUMETSAT aimed at refining the passband specifications of a post-EPS microwave sounder has recently concluded that negative impacts on forecast quality are detectable for channel frequency drifts greater than 1.5 MHz. This represents the uncertainty to which it is necessary to determine the channel passbands. Time did not permit a more detailed investigation during this preliminary assessment.

Figure 5 show the first guess departures, prior to bias correction, for MWTS and MetOp-A AMSU-A respectively. A comparison of these plots shows some interesting features. For MWTS Channel 1 the distribution is approximately 2K colder than for the equivalent AMSU-A channel (3). For MWTS channel 2 the peak of the distribution of first guess departures is colder than the equivalent AMSU-A channel (5) by approximately 0.6K, however, for both MWTS channels 1 and 2 the bias is relatively invariant with airmass, *i.e* the first guess departure field is approximately *flat*. This could be an artefact of the calibration process, for example in the antenna to brightness temperature corrections. In contrast, for MWTS channel 3 and 4 there is a stronger airmass-related bias, with more negative first guess departures in the tropics and more positive departures in the extra-tropics. In light of the discussion above on the apparent positive bias in MWTS channel 4 this appears surprising at first sight. Table 6, however, shows that the *assumed* passband specifications, for the purpose of generating RT coefficients, was displaced by 140 MHz relative to the nominal specification. In effect this displacement *over-corrected* the brightness temperature bias, causing a negative bias in the first guess departures. The equivalent AMSU-A channels (7 and 9) show much weaker airmass dependent biases. The large positive biases for MWTS channel 3 (0.5-1.0K) at 60° S in the eastern hemisphere are particularly striking. There are also large differences in first guess departures over land prior to bias correction. Despite these biases, the value of the data in an NWP data assimilation system depends largely on the ability of the bias correction scheme to eliminate these biases prior to assimilation.

Variational bias correction (VarBC, see Dee (2004)) was used to correct the FY-3A biases, using the same set of eight predictors used for ATOVS (one constant offset, four thickness based predictors and three related to scan angle for the correction of cross-track scan biases - see Table 7 and Table 8). The magnitude of the bias is shown for both MWTS and AMSU-A in Figure 6. These biases have been spun up over a period of 10 days.

Generally VarBC is applying larger bias corrections for MWTS than for AMSU-A. VarBC is having to work harder to eliminate the biases evident in the data and this is manifested as a larger spread in bias correction histograms. For all MWTS channels the signature of an airmass dependent bias is evident which is less evident in the AMSU-A corrections.

Figure 7 shows the first guess departures for MWTS and AMSU-A after bias correction. Clearly VarBC is significantly reducing the spread of the first guess departure fields for MWTS. For MWTS channels 3 and 4 a weak residual airmass dependent bias is still evident in the bias corrected departures which is less evident in the equivalent AMSU-A channels. This airmass dependent bias is most probably related to the remaining uncertainty in the channel passbands and, at several tenths of a Kelvin, is potentially significant. The demanding requirements for temperature sounding radiances makes the presence of these localised biases a concern, nevertheless the global first guess departure statistics are of sufficient quality to justify an assessment of the MWTS radiances in assimilation experiments.

3.1.2   Microwave Humidity Sounder (MWHS)

Figure 8 shows the first guess departure fields before bias correction for MWHS channels 1,3,4,5 - the 150 GHz window channel and the 183 ± 1, $\pm3,\pm7$ GHz water vapour sounding channels respectively. Channels 1 and 5 observed radiances exhibit negative biases relative to the modelled radiances whereas Channels 3 and 4 exhibit positive biases. Channels 3-5 show signs of a cross-track bias which can be difficult to fully correct using the existing VarBC scheme in which low order polynomials in the scan angle are used as predictors. Figure 8 also shows the same first guess departure fields after bias correction. The mean fields have been corrected effectively, but a residual scan bias remains. This is discussed in more detail in Sec 3.2 below. For comparison the equivalent first guess departure fields are also shown for MetOp-A MHS in Figure 8. The global departure statistics for MWHS are very similar to those for AMSU-B / MHS and of sufficient quality to assess the impact of the radiances on analysis and forecast accuracy.

3.1.3   Infrared Atmospheric Sounder (IRAS)

Figure 9 shows the first guess departures for a subset (channels 4-7) of the IRAS long wavelength CO_2 band temperature sounding channels, before and after bias correction. Also shown for comparison are the first guess departure fields for the equivalent MetOp-A HIRS channels. For channel 4 (centred at 703 cm^{-1}) with a weighting function peak at 400 hPa, the post-bias correction departure field shows residual localised positive biases around 60°S, 0°E of approximately +0.6K. This bias is not evident in the HIRS data for this cycle. Some sections of specific orbits also appear to exhibit biases quite different from adjacent orbits, see for example the section of orbit in the range 60°W - 120°W. The overall spread of the first guess departures is larger for IRAS channel 4 (standard deviation of 0.33 K) compared to HIRS (0.18 K). Post-bias correction standard deviations for all of the channels shown in Figure 9 (middle column) are larger by 60 % than the equivalent MetOp-A HIRS equivalents.

Figure 10 shows the first guess departures for channels 11 and 12 (water vapour sounding channels) and channels 14 and 15 (short-wave CO_2 channels) before and after bias correction respectively. Positive global biases for channels 11 and 12 are reduced, and made negative, by VarBC. The localised positive bias at 60°S, discussed above for channels 4-7, is also evident in these channels and is absent in the equivalent MetOp-A HIRS fields, also shown in Figure 10.

Localised biases in the higher peaking IRAS temperature sounding channels (1-3) have similar geographical distributions and are of larger amplitude. The correlation of these biases across several channels appears to support the hypothesis of an orbitally dependent calibration instability related to changing solar illumination and associated thermal cycling of the instrument around the orbit. Figure 11 shows the evolution of the local solar zenith angle with time for four orbits as well as temperature sensor data from the on-board blackbody. The blue shaded area indicates when the satellite is in Earth shadow (local night at the spacecraft location). The temperature sensor data shows that the temperature of this part of the instrument increases as the instrument emerges from shadow, and begins to drop prior to entering Earth shadow again. This thermal cycling is not necessarily a problem, but does indicate that there is thermal cycling in at least some components of the instrument. The middle panel of Figure 11 shows the evolution of first guess departures for IRAS channel 1 over the same period. Also shown is the derivative of the temperature sensor data (with respect to time) which exhibits a strong correlation (albeit lagged) with the first guess departure time series. The first guess departures are being used here as a proxy for the error in the measured brightness temperatures. The red shaded area shows where the first guess departures exceed a specified threshold and the periodicity of these regions support the hypothesis that the bias in the observed brightness temperatures is related to the thermal cycling of the instrument. The bottom panel of Figure 11 shows the evolution of the (derivative of the) temperature data for four of the

blackbody sensors illustrating that several parts of this component exhibit significant thermal cycling and may indicate that the black body is prone to thermal gradients.

Figure 12 compares the time series of first guess departures for IRAS and HIRS channels 1 to 4 over the course of two orbits. Large biases are evident in IRAS channels 1 and 2, but are more difficult to discern for channels 3 and 4 where the evolution of the departures is more complex. Similar biases are also evident for HIRS channels 1-3.

Further work is needed to establish whether the observed brightness temperature bias is caused by orbital thermal cycling. This work should consider the geometry of the instrument in relation to the spacecraft and should draw upon the full set of auxiliary data available from the instrument. The insights gained may help in the refinement of the instrument design for future FY-3 IRAS instruments. In the short term, a more detailed investigation will help in developing quality control schemes for the assimilation of data from the IRAS instrument.

3.2   Scan Biases

Figure 13 shows the scan biases for the MWTS, compared to those for the equivalent MetOp-A AMSU-A channels. This plot shows the mean bias correction averaged eight days. MWTS exhibits channel dependent cross track biases with peak-peak amplitudes in the range 1-3K. These are larger than the scan biases for the equivalent AMSU-A channels but these are generally well treated by the bias correction scheme. Residual biases are largest for channel 3 where the low order polynomial form of the cross track correction struggles to fully correct the more complex cross track bias pattern, but for channels 1, 2 and 4 the residual scan biases, *post-correction*, are as small as those for the equivalent AMSU-A channels.

Figure 14 shows the scan biases for the MWHS, compared to those for equivalent MetOp-A MHS channels. Here the dominant component of the scan bias, for channels 1-4, is a complex modulation across the swath with a peak-peak amplitude in the range 0.5 to 2 K. The low order polynomial (in scan angle) bias predictors are unable to deal adequately with this form of cross track scan bias and consequently biases are evident even after bias correction. Such biases have been observed in other instruments, for example in NOAA-19 AMSU-A channel 7 (Bormann (2009)) and present difficulties for the existing ECMWF bias correction scheme. Possible solutions to this problem would be to implement a scan position dependent offset in the pre-processing of the radiances, using values derived from this study, or to implement a scan position dependent predictor in VarBC.

Figure 15 shows the scan biases for a subset of the IRAS channels, compared to those for the MetOp-A HIRS equivalent channels. For the temperature sounding channels shown here (4-7) it can be seen that although the corrections applied are relatively large, as large as 3.5K for channel 4 for example, the bias corrected radiances show no significant residual biases across the swath after correction. The corrections applied for these channels are, however, significantly larger than those applied to the equivalent HIRS channels, which are generally below 0.5K for these channels. For channels 11, 12 (water vapour sounding channels), 14 and 15 (short wave temperature sounding channels) the bias corrections applied to the IRAS channels are as large as 2K, significantly larger than the corrections applied to the equivalent HIRS channels (generally less than 1K for these channels). Nevertheless the bias correction is effective in reducing the mean IRAS bias to below 0.2K for these channels.

Figures 16 and 17 show the scan biases for the MWRI and AMSR-E respectively. For all MWRI channels, although the bias correction applied is quite large in some cases (*eg.* -10K for the 23 GHz (H) channel) the correction is relatively constant across the swath, indicating an absence of any spacecraft obstructions in the radiometer field of view. Likewise the bias corrections applied to the AMSR-E data are relatively constant across the swath and, in some cases, of relatively large amplitude (*eg.* 23.8GHz (H) which has a correction of 3K applied). A likely explanation for the large biases for these channels is errors in the conversion of

antenna temperatures to brightness temperatures which takes account the effects of feed-horn spillover effects and cross polarisation contamination. Both of these are dependent on accurate pre-launch characterisation of these effects, which is difficult to achieve.

3.3   Data Quality: First Guess Departure Statistics

An overview of the data quality for the key channels of the four FY-3A instruments, in terms of the standard deviations of the first guess departures, is given in Figure 18. Also shown for comparison are the equivalent statistics for the corresponding MetOp-A instruments and, for the case of the MWRI instrument, the equivalent AMSR-E statistics. The statistics have been obtained over 1 month. These statistics measure the fit of the ECMWF model to the measured radiances and give a good early indication of data quality as any gross errors in the data would be manifested as a large spread in the first guess departures

Figure 18a shows a comparison for MWTS/AMSU-A. The standard deviation for MWTS channels 3 and 4 (0.25-0.26K) are significantly larger than those for AMSU-A channels 7 and 9 (0.2-0.21K). There are several possible reasons for this: firstly, as discussed in Section 3.1.1 residual localised biases caused by uncertainties in the channel passbands would be expected to increase the global standard deviation. Secondly, the specified NEΔT for these channels (0.4K) is larger although it is noteworthy that the on-orbit performance of the instrument is significantly better than this and is probably in the range 0.23-0.25K.

Figure 18b shows the comparison for MWHS/MHS for the 183 GHz water vapour sounding channels. The standard deviations for the MWHS channels are around 15% larger than the MHS channels, most probably due to the complex scan biases which are not dealt with well in the current VarBC scheme.

The comparison for IRAS/HIRS is shown in Figure 18c. For the temperature sounding channels (4-7, 703-749 cm^{-1}) the standard deviations of the first guess departures for IRAS are 50-70% larger than the corresponding HIRS channels, as a result of the orbital biases discussed in Section 3.1.3.

The comparison of the MWRI with AMSR-E, valid for the period 10-17th September, is shown in Figure 18d. MWRI compares well with AMSR-E for most channels, and is similar in quality to AMSR-E with standard deviation of first guess departures up to 25% larger than the equivalent AMSR-E channels.

Histograms of background departures for the three sounding channels of the MWTS (channels 2-4) are shown in Figure 19 (top panel). Also shown for comparison are the statistics from the equivalent channels for NOAA-18 AMSU-A obtained for the same period. The fit of the measured MWTS radiances to the model is better than 0.3 K (standard deviation, shown in Figure 18a), only slightly larger than the equivalent AMSU-A statistics. The larger standard deviations are to be expected and result from the higher noise levels in the MWTS measurements.

Histograms for the background departures for the MWHS are also shown in Figure 19 lower panel alongside equivalent histograms for the MetOp-A MHS instrument. The MWHS data is similar in quality to the MHS data and was judged to be of sufficient quality to include in assimilation experiments. Analyses of the IRAS data exposed some orbital biases in the highest peaking temperature sounding channels (1-3). However, the departure statistics for the channels equivalent to HIRS channels currently used in operations, not shown here, showed the data to be of only slightly inferior quality.

Histograms of background departures for the MWRI channels are shown in Figure 21. Also shown for comparison are the departures for the equivalent channels of AMSR-E. Due to mechanical interactions with the platform the MWRI has been activated only intermittently and the dataset is therefore relatively sparse, thereby preventing a meaningful assessment through assimilation experiments.

3.4 Data Quality: Stability

A subset of the FY-3A data, covering the period 20 July 2008 - 1 November 2008, was available for assessment in the IFS. Despite this representing a fairly short period of time, it highlights any periodic or episodic changes in data quality or volume. Inspecting the time evolution of departure statistics is used here to assess the stability of the data stream in terms of data volume and quality as well as to diagnose the performance of the bias correction scheme. When used in near-real time mode this type of analysis can yield very useful feedback to satellite agencies on the impacts of any changes to the on-orbit configuration of an instrument or changes to the ground segment processing of the data stream.

Figure 22 shows the mean (and the standard deviation) of the first guess departures for the MWTS channel 2, standard deviations are also shown for channels 3 and 4. For the periods before and after a ground segment processing change on 16th August 2008, the radiances for channels 2 and 3 appear to be stable, with no significant trends over these periods. The ground segment change to the pre-processing system resulted in a shift of approximately 0.8K for channel 2. Also noticeable is a regular data outage around the last day of each month, causing transient spikes in the means and standard deviations for all MWTS channels.

Figure 23 shows the evolution of the VarBC coefficients over the period 20th July - 9th October. The plot illustrates that following the ground processing change on 16th August the bias correction scheme adapts within 5-10 days and thereafter the bias corrections are relatively stable. Some instability is evident around the periods of data drop-outs, which is to be expected.

Figure 24 shows the mean (and the standard deviation) of the first guess departures for the MWHS channel 3 as well as standard deviations for channels 4 and 5. In common with MWTS, data drop-outs are noted at the end of each month. In addition, a significant change was implemented, as part of a ground processing software update, at the end of August 2009. This change dealt largely with some *striping* effects evident in earlier versions of the MWHS data. The change is manifested as discontinuities in the bias for channel 2 and in the standard deviation for channel 5. Figure 25 shows the evolution of the bias correction coefficients for MWHS channels 3 (183$\pm$1 GHz). The response of VarBC following the major change at the end of August is evident, particularly in the offset coefficient ($p(0)$), but the other coefficients are still evolving, albeit slowly, for the remainder of the period.

Figure 26 shows the mean (and the standard deviation) of the first guess departures for the IRAS channel 5 as well as standard deviations for channels 11 and 14. These channels were selected to be representative of the IRAS temperature sounding channels (channel 5 at 716 cm^{-1})), the moisture sounding channels (channel 11 at 1365 cm^{-1}) and the short-wave CO_2 channels (channel 14 at 2210 cm^{-1}). Figure 27 shows the associated evolution of the VarBC coefficients for channels 5 and 11. Prior to a ground processing system change on 31st July 2009 the VarBC coefficients are changing rapidly. Following the change, the channel 5 coefficients converge within 10 days and are relatively stable thereafter. The channel 11 coefficients exhibit a slow drift for the remainder of the period. The evolution of the bias and standard deviations in 26 are consistent with these changes and show additional transient spikes, associated with a 2 day data outage, during the 14-15th September.

For MWRI, assessing stability was more difficult due to the intermitent operation of the instrument.

Figure 28 shows the evolution of the mean first guess departures for MWRI channel 3 during the period 10-17 September 2008 also shown are the standard deviations of the first guess departures for channels 3,5 and 7. Figure 29 shows the associated evolution of the VarBC coefficients demonstrating reasonably fast convergence, even over such a short period of time.

4 Observing System Experiments

4.1 Introduction

Observing system experiments (OSEs) are commonly used as a means of assessing the value of new observational datasets in NWP data assimilation systems. Recent examples include the work at ECMWF to assess the influence of the main humidity observing systems (Andersson et al. (2007)) and the impact of microwave imager data in NWP (Kelly et al. (2008), Geer et al. (2008)). An approach commonly used to assess the value of new data sources is to add data to an *observation depleted* observing system. In such a system, analysis and forecast errors are larger than might be expected from a *full* observing system. Consequently, the improvement in analysis and forecast accuracy are larger than would be the case for a full observing system. The larger signals in forecast skill measures thereby facilitate a comparison of a new data type with other similar observation types. This type of experiment provides a check that there are no serious problems with a new observational data type. These baseline experiments, of course, do not give a realistic representation of the forecast improvement to be expected when the new data is added to a full system. Full system experiments are conducted to assess the impact of new data types when analysis errors are small, and are normally carried out in the later stages of pre-operational testing. In the context of the evaluation of FY-3A data the purpose of full system experiments is to check that the new data does not cause any measurable degradation to forecast performance. Both *baseline* and *full system* experiments are described in Sections 4.2 and 4.3 below.

4.2 Baseline Experiments

Initial baseline experiments were run at low resolution (T159) to assess the impact of the individual FY-3A instruments relative to that from the equivalent NOAA/MetOp instruments against an *observation depleted* control experiment. Subsequently, higher resolution (T511) baseline experiments were run to assess the impact of the VASS suite of instruments (MWTS, IRAS, MWHS) relative to the ATOVS suite of instruments on MetOp-A. Both sets of experiments are described below.

4.2.1 Baseline Experiments at T159 Resolution: Assessing the Impact of Individual Instruments

The control chosen for these experiments included a depleted observing system in which only conventional observations, observations from F13 and F15 SSMI as well as data from six GPSRO sensors were included in the analysis. GPSRO bending angle data are assumed to have very low absolute measurement uncerainties and are assimilated without bias correction. This effectively anchors the variational bias correction system, ensuring that long term drifts in model bias are prevented. Recent OSEs have shown that GPSRO satellite provide a powerful constraint on the large scale analyses (S. Healy, *pers. comm.*), and results in forecast impacts close to that from IASI in the southern hemisphere. Overall, in the Southern Hemisphere GPSRO data provides around 50% of the impact of a full observing system relative to a *conventional observations only* control experiment. The control configuration chosen here is therefore a reasonable choice. MWTS, MWHS, IRAS and equivalent MetOp-A ATOVS instruments were added separately to this control experiment:

- **Control:** conventional observations + SSMI + GPSRO

- **Baseline1:** Control + FY-3A MWTS

- **Baseline2:** Control + MetOp-A AMSU-A (5,7,9)

- **Baseline3:** Control + FY-3A MWHS

- **Baseline4:** Control + MetOp-A MHS

- **Baseline5:** Control + FY-3A IRAS

- **Baseline6:** Control + MetOp-A HIRS

The experiments were run for the period 20th August 2008 - 1st October 2008 and the resulting forecast verified against operational analyses. Observation errors for the FY-3A instruments were determined by scaling the observation errors for the equivalent ATOVS instruments by the ratio of the standard deviations of the first guess departures from MWTS and AMSU-A. Only channels 5,7 and 9 from MetOp-A AMSU-A were assimilated to provide as near to a *like-for-like* comparison as possible.

As a summary of the impacts, the resulting anomaly correlation scores (500 hPa Geopotential) and RMS errors for humidity for these experiments are summarised in Figure 31. Relative to the control, the FY-3A MWTS shows significant forecast skill impact, amounting to 70% of the impact of AMSU-A at Day 4 in the SH. The impact for IRAS is positive, but smaller than for MWTS, amounting to 20% of the impact of MetOP-A HIRS at day 4. This may be partially attributable to the residual biases in the bias corrected IRAS data. The MWHS shows very similar impact to that from MetOp-A MHS, with measurable improvements to humidity forecast to Day 3. The first guess departure statistics of Baseline3 from 28 September to 28 October 2008 are shown in Figure 30 to demonstrate the impact of assimilating FY-3A MWHS on the first guess departure fits for radiosonde observations in the Tropics and SH and Dropsonde fits in the NH. First guess departure fits for humidity are generally improved for the 200-700hPa levels.

4.2.2 Baseline Experiments at T511 Resolution: Assessing the Impact of the VASS Instrument Suite

The control experiment here used data from a single AMSU-A in order to provide some constraint on the background fields. Data from NOAA-18 was used as this satellite was in an orbit orthogonal to the FY-3A platform. This meant that FY-3A data was influencing the analysis at different locations to the NOAA-18 data, with the NOAA-18 data providing some control on the quality of the analysis. The following experiments were run over the period 20 July - 1 November 2008:

- **Control:** conventional observations + NOAA 18/AMSU-A + ozone data + scatterometer data

- **Baseline1:** Control + MetOp-A AMSU-A (ch.5, 7, 9) + MHS + HIRS)

- **Baseline2:** Control + FY-3A (MWTS + MWHS + IRAS)

The results, in terms of the anomaly correlation of the forecasts in the NH and SH over the period 30 July to 1 November 2008 are shown in Figure 32. In the NH the impact of the FY-3A data is very similar to that from the MetOp-A instruments. In the SH the impact is, for forecast ranges to day 7, positive for the FY-3A data and a significant fraction of that obtained from MetOp-A.

First guess departure statistics for radiosonde observations in the NH, TR and SH for the Baseline2 experiment from 20 July to 30 October 2008 are shown in Figure 33 to demonstrate the impact of assimilating FY-3A VASS on the short range forecasts of humidity. FY-3A data significantly improves the first guess humidity fields in the Tropics and SH. Impacts are smaller in the NH. This is a very encouraging result.

4.3   Full System Experiments

A full system experiment was run over the period 20080720-20081101, using a T511 configuration of the operational model. The suite of FY-3A sounding instruments (MWTS, MWHS and IRAS) were added to the full ECMWF system. The OSEs carried out were therefore:

- **FULL SYSTEM 1:** CY35R2 full system experiment

- **FULL SYSTEM 2:** CY35R2 full system experiment + FY-3A (MWTS + MWHS + IRAS)

The forecast verification results are summarised in Figure 34. Overall the impact of the FY-3A instruments is close to neutral, with some positive impacts in the NH for forecast ranges beyond Day 3 for which the improvments appear statistically significant at the 90% level. This is an encouraging sign as full system experiments are a demanding test of data quality. Figure 35 shows zonal mean plots of forecast error differences (Full System 1 - Full System 2) for geopotential height. The results are overall consistent with the summary plots in Figure 34.

The first guess departure statistics of Baseline2 from 20 July to 30 October 2008 are shown in Figure 36 to demonstrate the impact of assimilating FY-3A VASS on the first guess fits for MetOp-A AMSU-A (NH) and MHS (SH). Impacts are neutral for MetOp-A AMSU-A, but fits for MetOp-A MHS are improved.

5   Summary, Conclusions and Further work

Data from the FY-3A VASS instruments as well as the microwave imager (MWRI), obtained during the July-November 2008 Calibration-Validation phase of this preparatory mission, have been introduced into the ECMWF Integrated Forecasting System. This has permitted an assessment of data quality through an analysis of first guess departure statistics, a comparison with equivalent ATOVS instruments, as well as through observing system experiments. The use of NWP model fields for the calibration and validation of satellite missions is becoming standard practise as the global coverage and high accuracy provided by NWP models have been proven to be a powerful tool in the diagnosis of systematic biases in the data, and this has again been the case with the assessment presented here. The assessment of the data through OSEs provides, in addition, valuable information on the impact of the data on NWP analysis and forecast quality.

In the OSEs presented here the individual VASS instruments (MWTS, MWHS and IRAS) were able to show significant positive impact, equivalent to a significant fraction of the impact from the equivalent MetOp-A ATOVS instruments when assimilated in a *like-for-like* configuration. As a *package* the VASS instruments show impact equivalent to a significant fraction (*e.g.* ~ 30% at day 5 in SH 500hPa geopotential height anomaly correlation) of that obtained from the MetOp-A ATOVS suite, even when added on top of a control experiment with one AMSU-A. When added to a full observing system OSE the impact of the FY-3A data is neutral to slightly positive, a result which is encouraging and indicates that there are no *major* problems with the data from FY-3A from an NWP perspective. Overall the results from these OSEs, using data from the Cal/Val phase of this preparatory mission, are a very promising start to the FY-3 program.

Perhaps more importantly, this assessment has highlighted several issues where further work needs to be done to refine the instrument design and pre-launch testing as well as the ground processing systems, in order to further improve the quality of FY-3 data for FY-3A and subsequent missions. In order of significance these are:

- **Uncertainties in MWTS passbands.** This initial assessment has presented evidence that the passband for channel 4 of the MWTS instrument is shifted by ~ 100 MHz relative to that for the pre-launch design

specification, and ~ 50 MHz relative to pre-launch measurements. This uncertainty leads to an airmass dependent bias which is only partially compensated for by VarBC. Further work is needed to establish the on-orbit passband centre frequencies and bandwidths for all MWTS channels and determine if there is any temporal or orbital evolution of the shift. Independent studies have recently shown that uncertainties of 1.5 MHz or less are required in the specification of band centres in order to render the effects negligible on NWP forecast accuracy.

- **Orbitally dependent biases in the IRAS observations.** Channels 1-3 show orbitally dependent biases that are probably correlated with the solar induced thermal cycling of the instrument. For channel 1 the effect is locally as large as 10 Kelvin. There is some indication that these biases affect other channels as well. Further work should establish the cause of these biases, in order that improvements can be made in future FY-3 instruments, if appropriate. A more detailed study on the impact for channels 4-7 would be worthwhile.

- **Scan biases for MWHS.** The water vapour sounding channels exhibit complex cross scan biases which are difficult to correct in the present ECMWF VarBC scheme. These biases, in the short term, would be best dealt with a pre-processing step or by a modification of the VarBC predictor scheme to include field of view dependent offsets. In the longer term, perhaps for future instruments, it would be beneficial to eliminate the cause of the cross scan bias problems.

- **Biases in sections of the IRAS orbit.** Sections of IRAS orbit were found to exhibit biases different from adjacent orbits and other parts of the same orbit. This is distinct from the orbital biases described above. This particular type of error is not handled well using VarBC and therefore more work is required to identify the cause of these biases and to develop methods for screening this data.

- **Offsets in the brightness temperatures for all VASS instruments and the MWRI instrument.** Although these types of errors can generally be dealt with effectively using VarBC, there are some climate related applications of the data that would benefit from smaller absolute uncertainties in the measured brightness temperatures. For MWRI, for example, the biases in some channels are in the range 5-10K. This may be a result of uncertainties in the antenna to brightness temperature corrections applied to date, which may require further tuning. For future missions, improved characterisation pre-launch would be a better solution.

- **Data Outages.** The regular data outages at the end of each calendar month do not present a serious problem for the use of the data in NWP and are doubtless the consequence of early Cal/Val phase tuning of the ground segment, however it would be beneficial to eliminate these for future data streams before further OSE's are performed.

One important lesson from this study, also drawn from experience of POES, MetOp and DMSP missions, is that early assessment of the data using NWP systems is a valuable component of the calibration and validation of satellite missions. Early data access ensures that instrument issues can be flagged early and mitigation measures put in place in time for subsequent launches. Useful feedback can also be generated by NWP centres on the impact of changes to the ground processing systems or instrument configuration during the early orbit commissioning phase of a mission. A related benefit for NWP centres is that processing systems are developed and tested at the earliest possible opportunity, hence maximising the benefit extracted from the data. The processing systems for FY-3A and FY-3B will be available with the release of CY36R4, due to become operational in Autumn 2010.

Acknowledgments

Figure 1: Coverage for the FY-3A MWTS instrument in relation to other AMSU-A instruments currently assimilated at ECMWF, colour-coded by satellite. Data is taken from the 6-hour period around 20 September 2008 00Z. For clarity, not every available field of view is plotted.
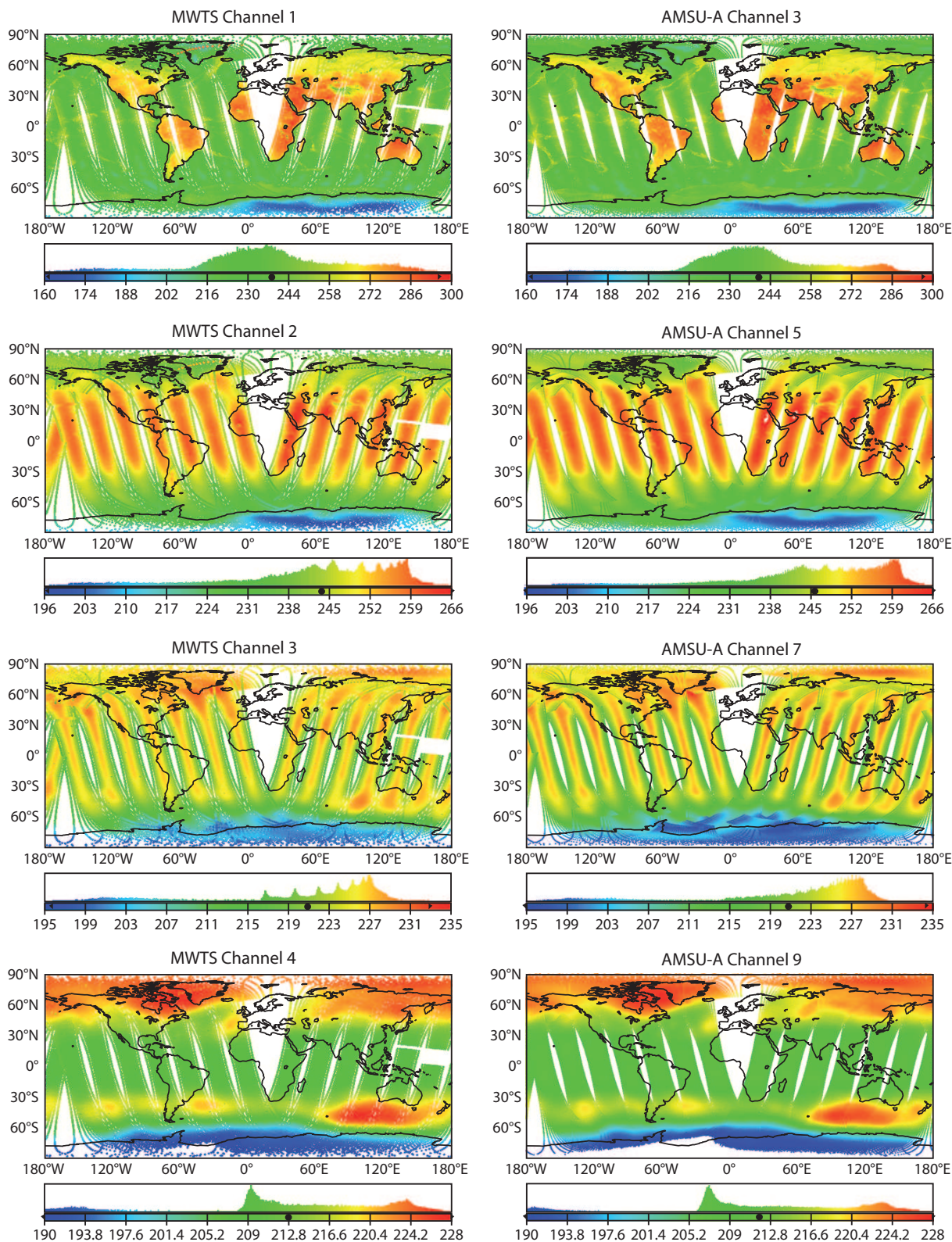
Figure 2: *Observed brightness temperatures for FY3-A MWTS and the equivalent MetOp-A AMSU-A channels. The left column shows the observed brightness temperatures for FY3-A, the right column shows brightness temperatures for the equivalent MetOp-A AMSU-A channels (for cycle 2008091700). The spot at the base of the histograms indicates the mean brightness temperature for each plot.*
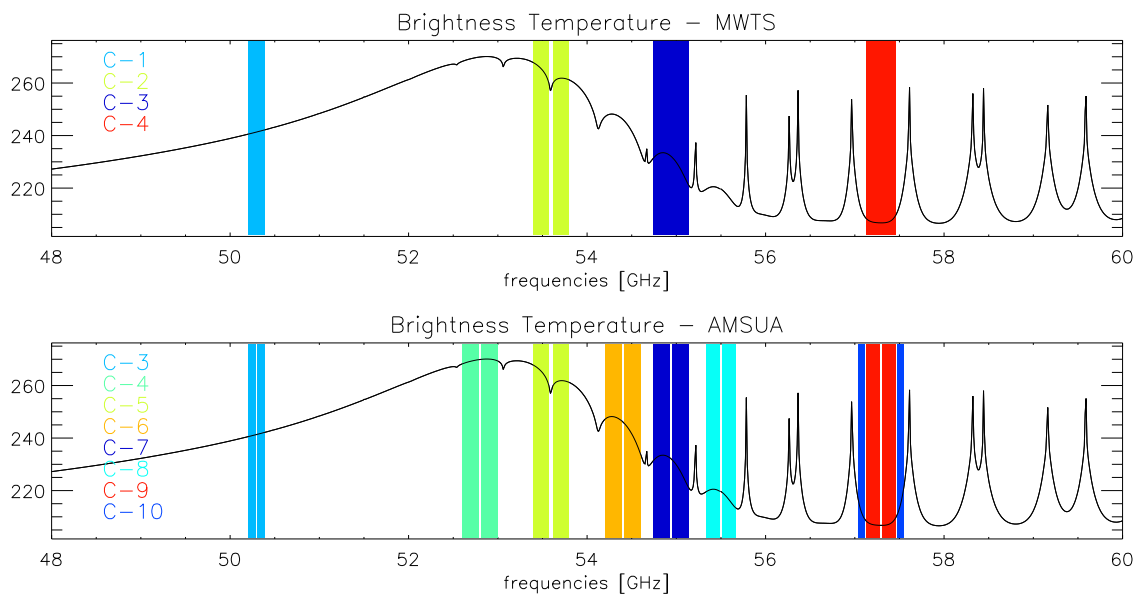
Figure 3: Brightness temperatures for a typical atmospheric profile in the 48-60 GHz region showing the passbands for MWTS channels 1-4 and (top) and AMSU-A channels 3-10 (bottom).
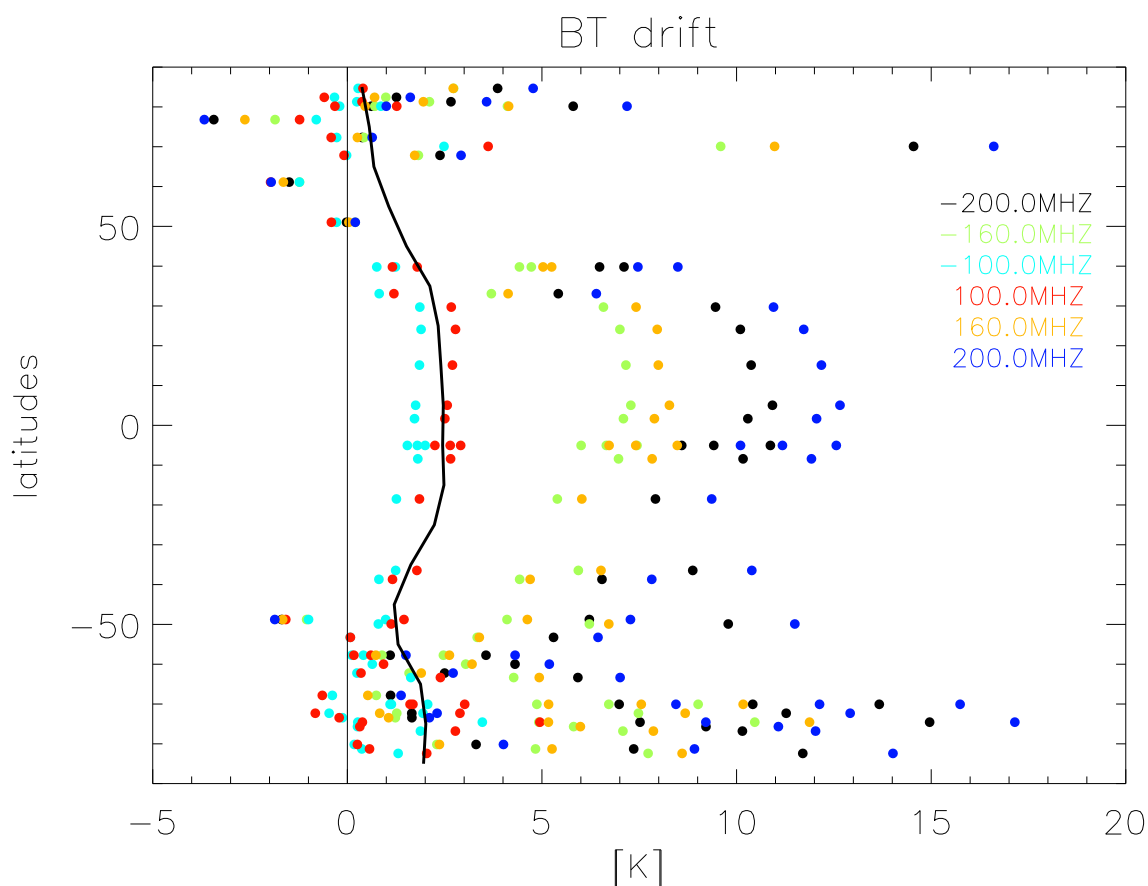
Figure 4: The effects of passband shift for MWTS channel 4. The black line shows the latitudinally-averaged brightness temperature difference between FY-3A MWTS channel 4 and MetOp-A AMSU-A channel 9 (the proxy *for the true brightness temperature). The coloured dots show the simulated brightness temperature error resulting from specified frequency shifts relative to the nominal passband specification (centre at 59.29 GHz, with a bandwidth of 330 MHz). The brightness temperatures were simulated by a microwave line-by-line model using 52 diverse atmospheric profiles. The horizontal axis represents the brightness temperature errors in Kelvin.*
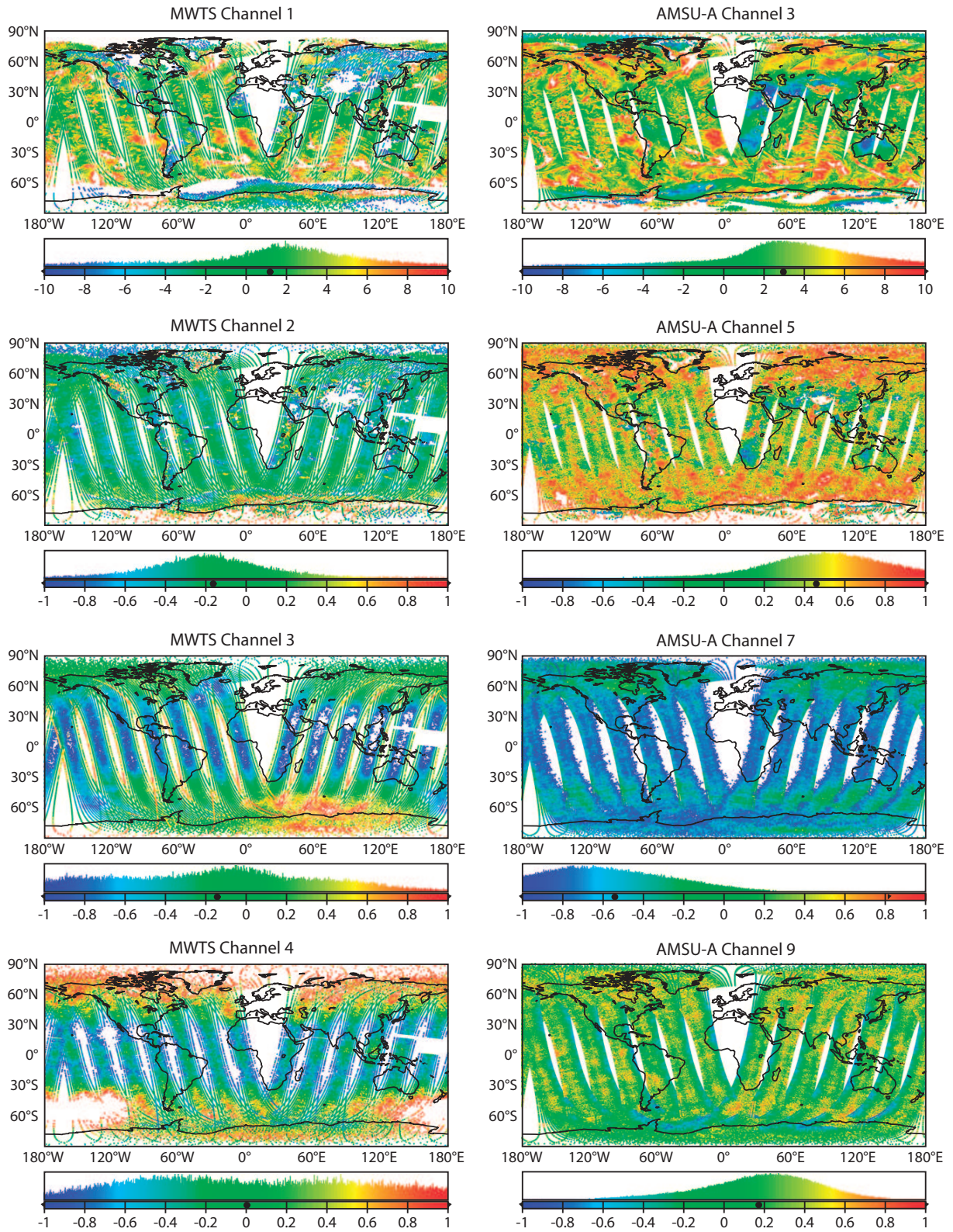
Figure 5: Comparison of first guess departures, before bias correction, for FY3-A MWTS (left column) and the equivalent MetOp-A AMSU-A channels (right column) at cycle 2008091700.
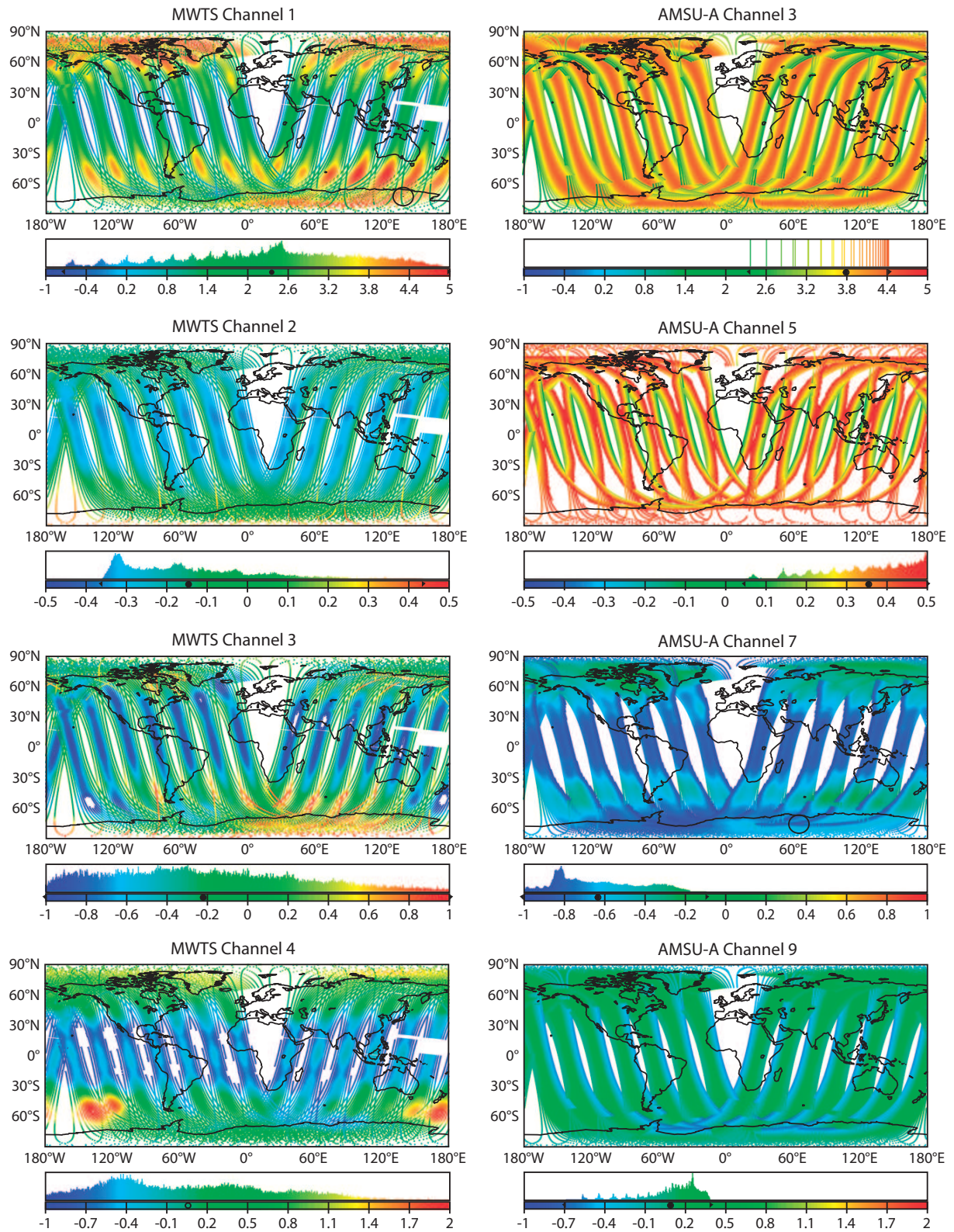
Figure 6: Comparison of bias corrections for FY3-A MWTS (left) and the equivalent MetOp-A AMSU-A (right) at cycle 2008091700.
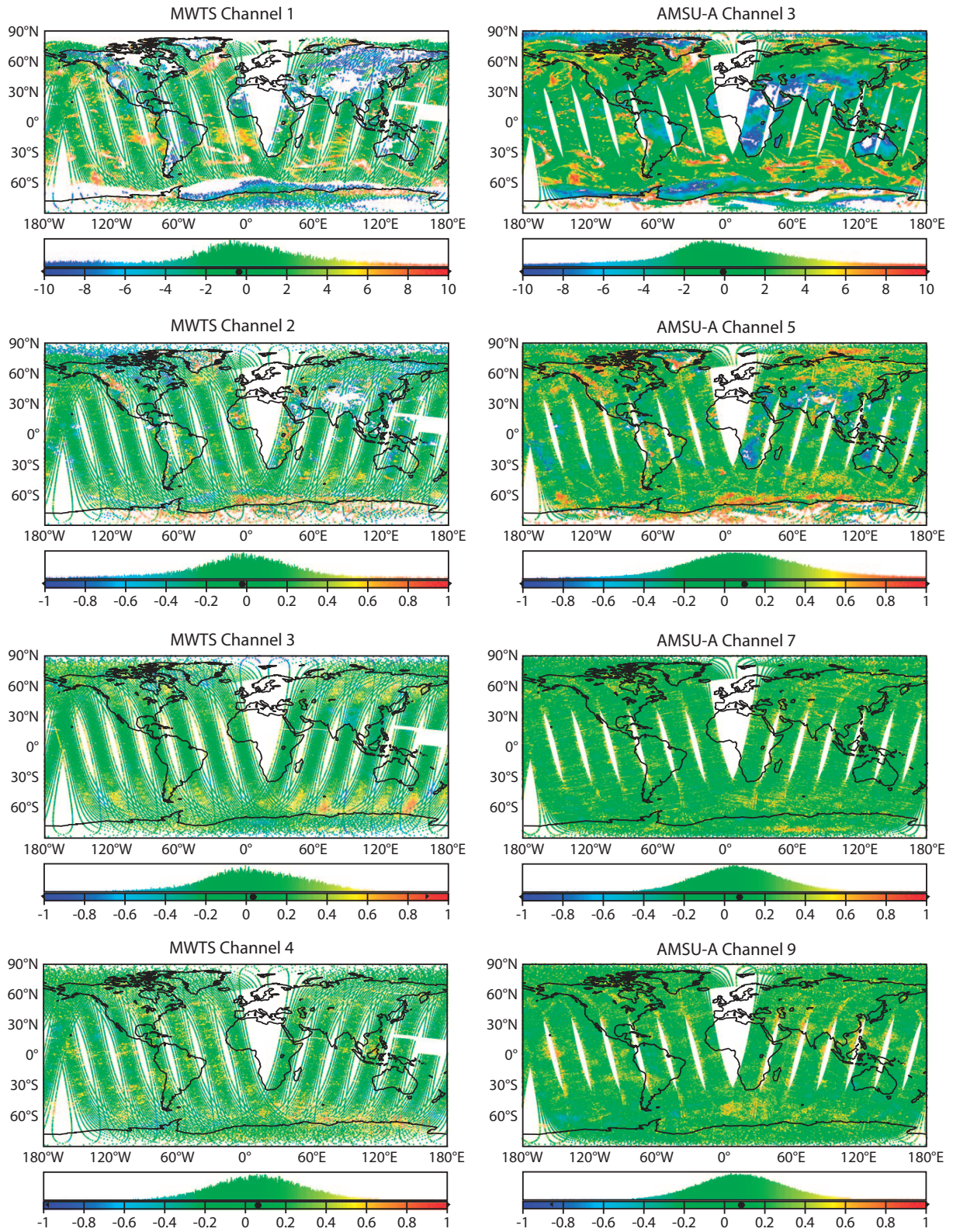
Figure 7: Comparison of first guess departures, after bias correction, for FY3-A MWTS (left column) and the equivalent MetOp-A AMSU-A (right column) at cycle 2008091700.
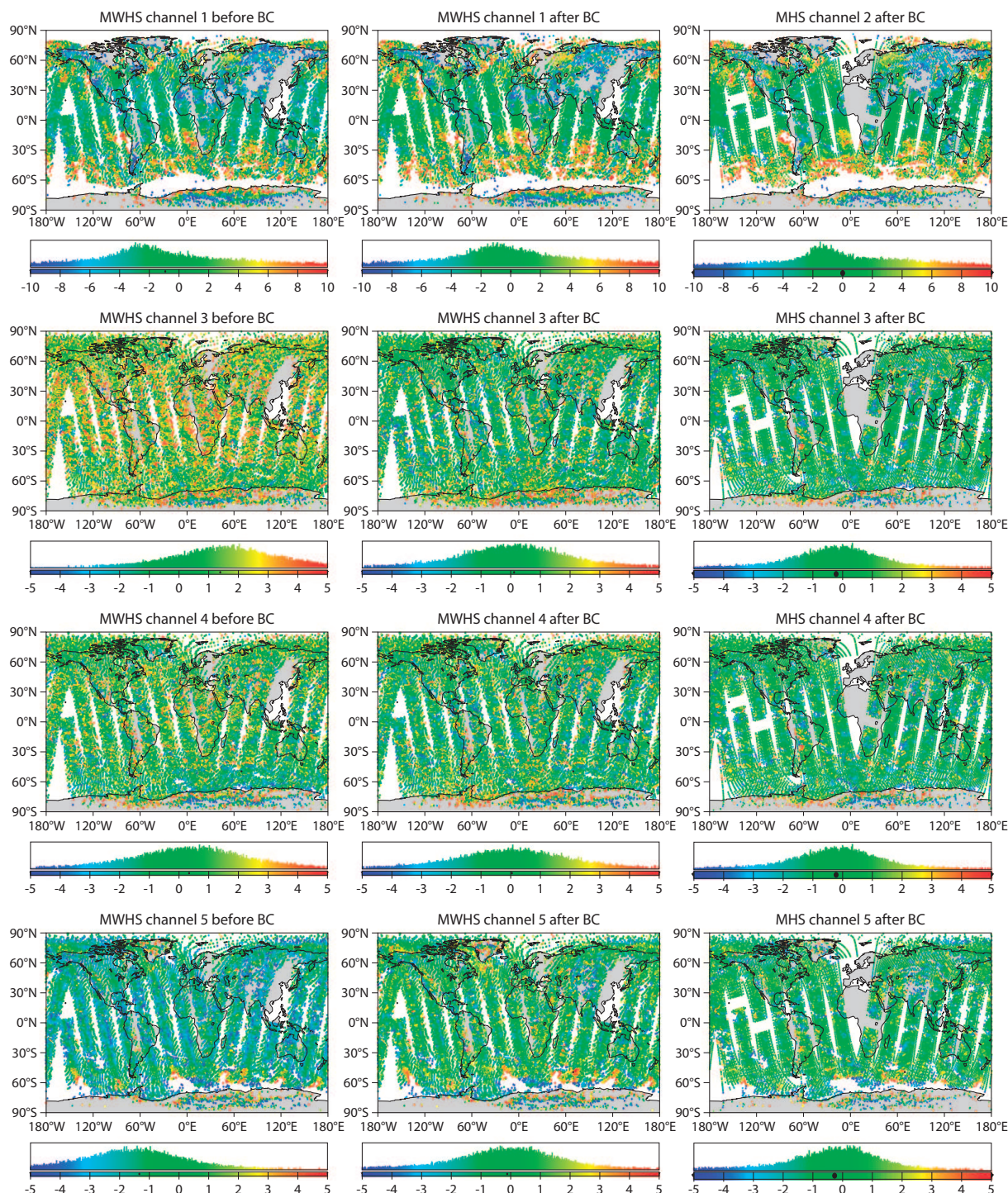
Figure 8: First guess departures for FY3-A MWHS (before and after bias correction) and MetOp-A MHS (after bias correction) at cycle 2008091700.
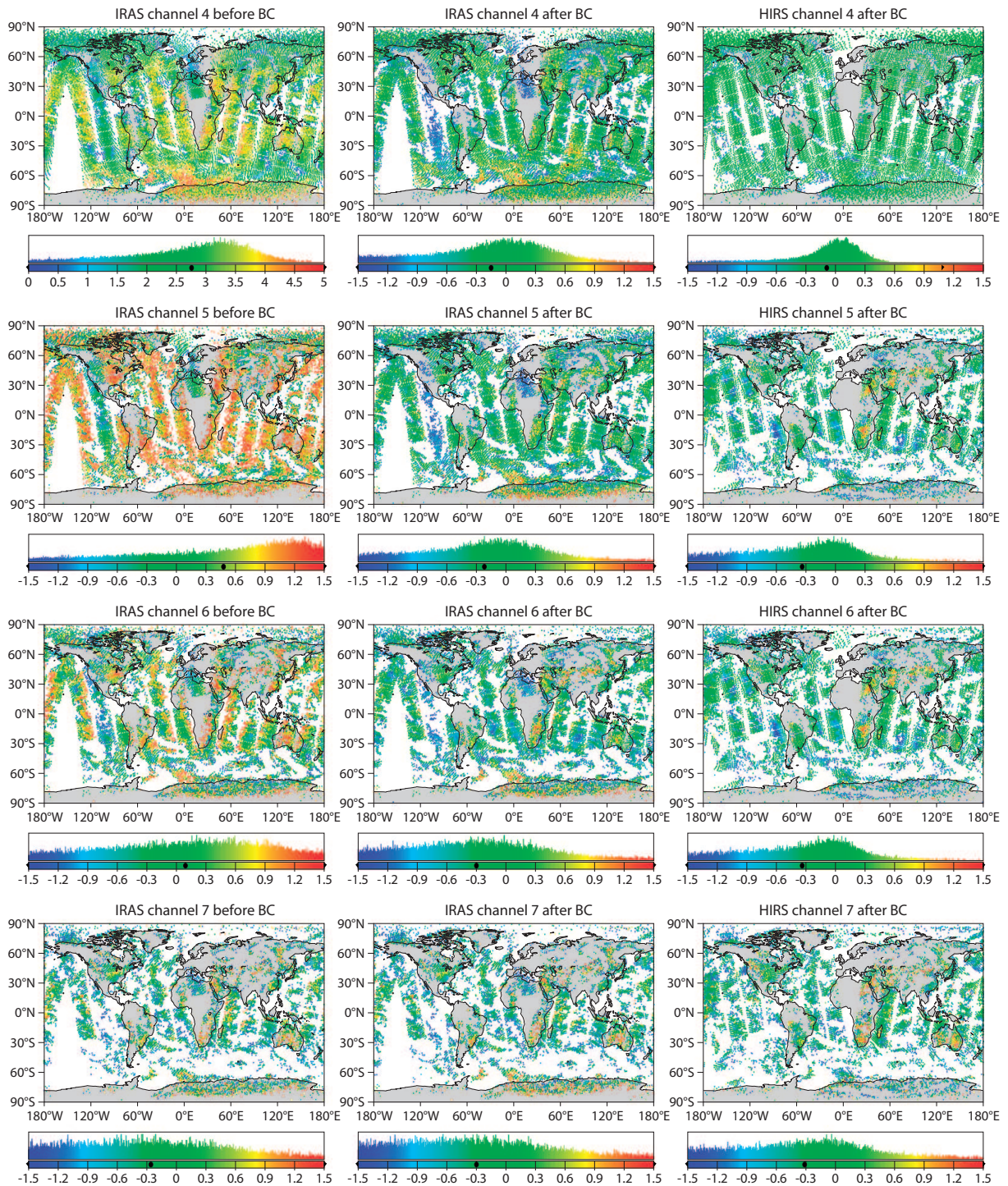
Figure 9: First guess departures for FY3-A IRAS before (left) and after (centre) bias correction, and MetOp-A HIRS (right). First guess departures are shown for the temperature sounding channels that are currently used in operations (channels 4-7), at cycle 2008091700).
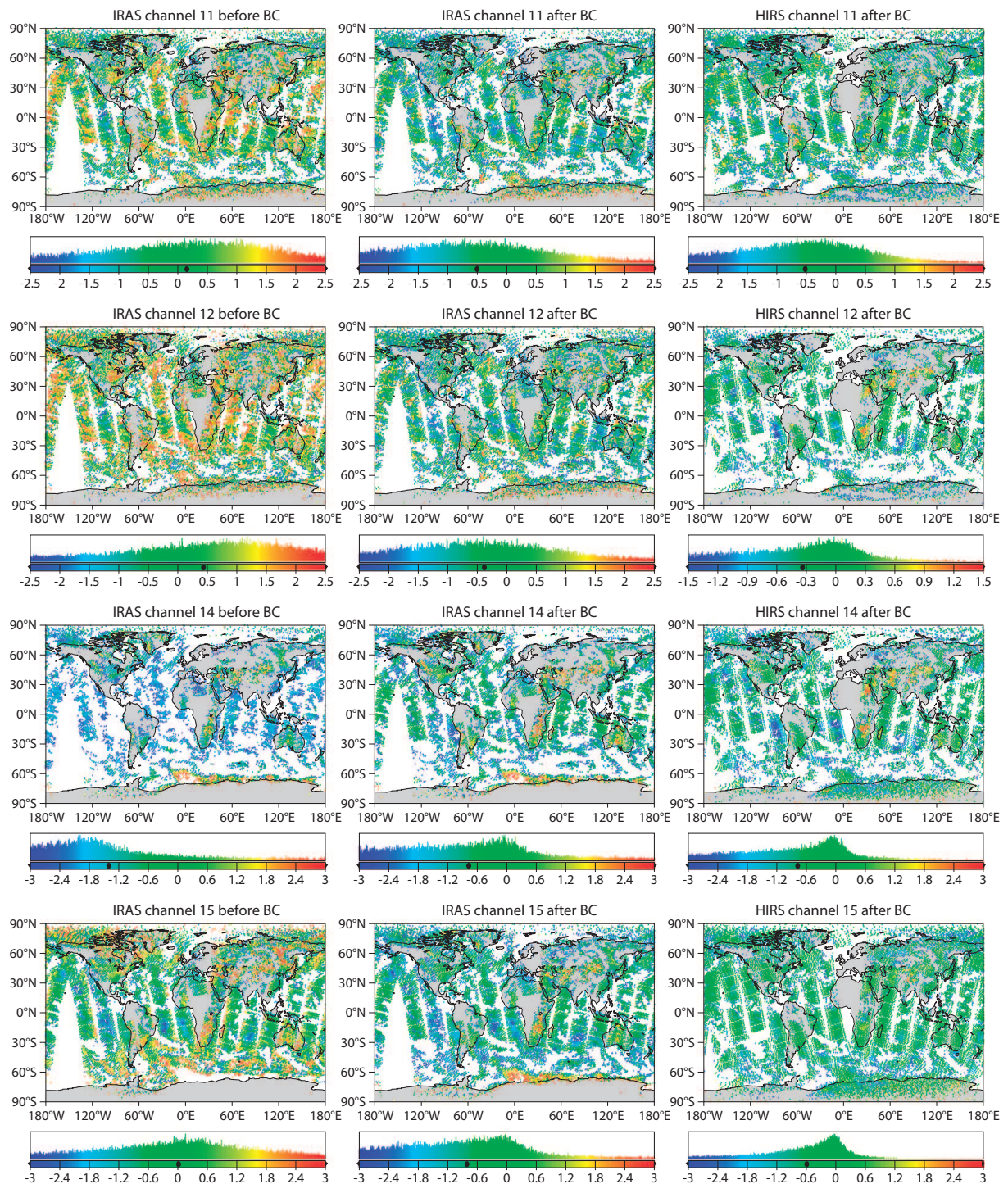
Figure 10: First guess departures for FY3-A IRAS before (left) and after (centre) bias correction, and MetOp-A HIRS (right). First guess departures are shown for water vapour sounding channels (11 and 12) as well as short wave temperature sounding channels (14 and 15), at cycle 2008091700
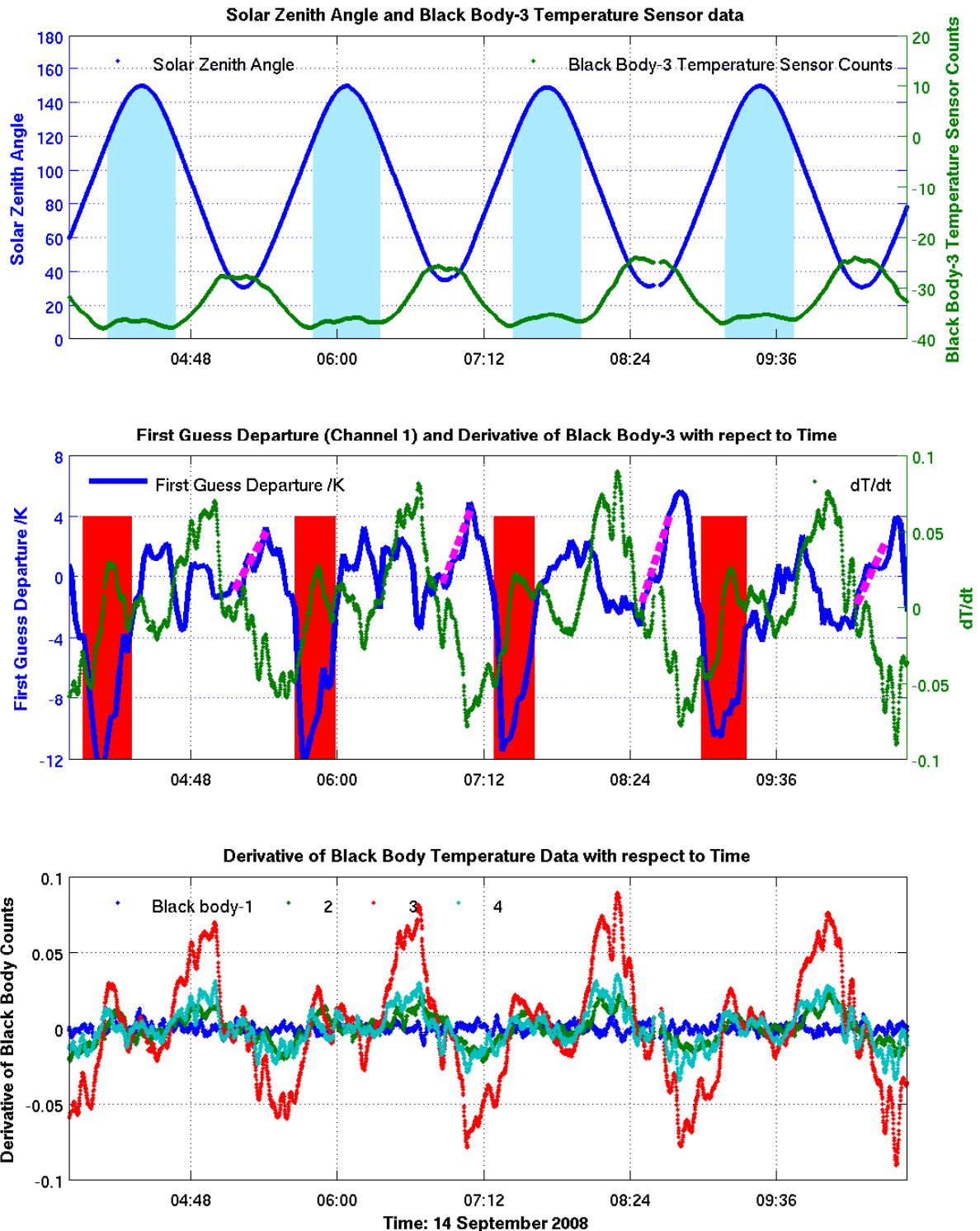
Figure 11: Orbital biases in IRAS channel 1. The top panel shows the solar zenith angle against time and temperature sensor counts of black body (sensor 3) the blue shaded areas indicate part of the orbit where the spacecraft is in earth shadow (ie local night); the middle panel shows the first guess departure before bias correction (blue curve) and the derivative of the black body temperature with respect to time; the bottom panel shows the derivative of black body temperature sensors with respect to time.
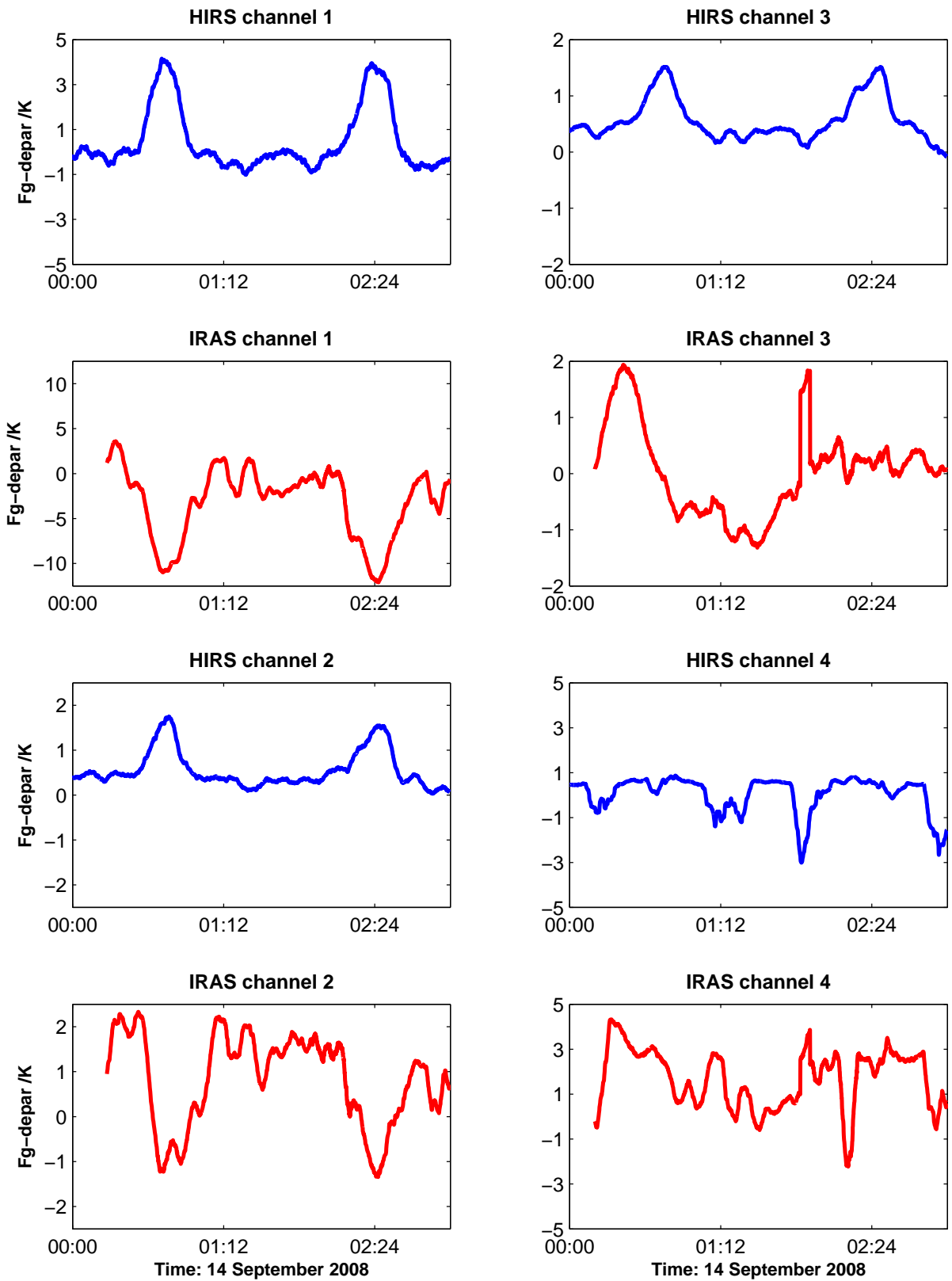
Figure 12: The time series of standard deviations of first guess departures, before bias correction, for IRAS and HIRS channels 1-4.
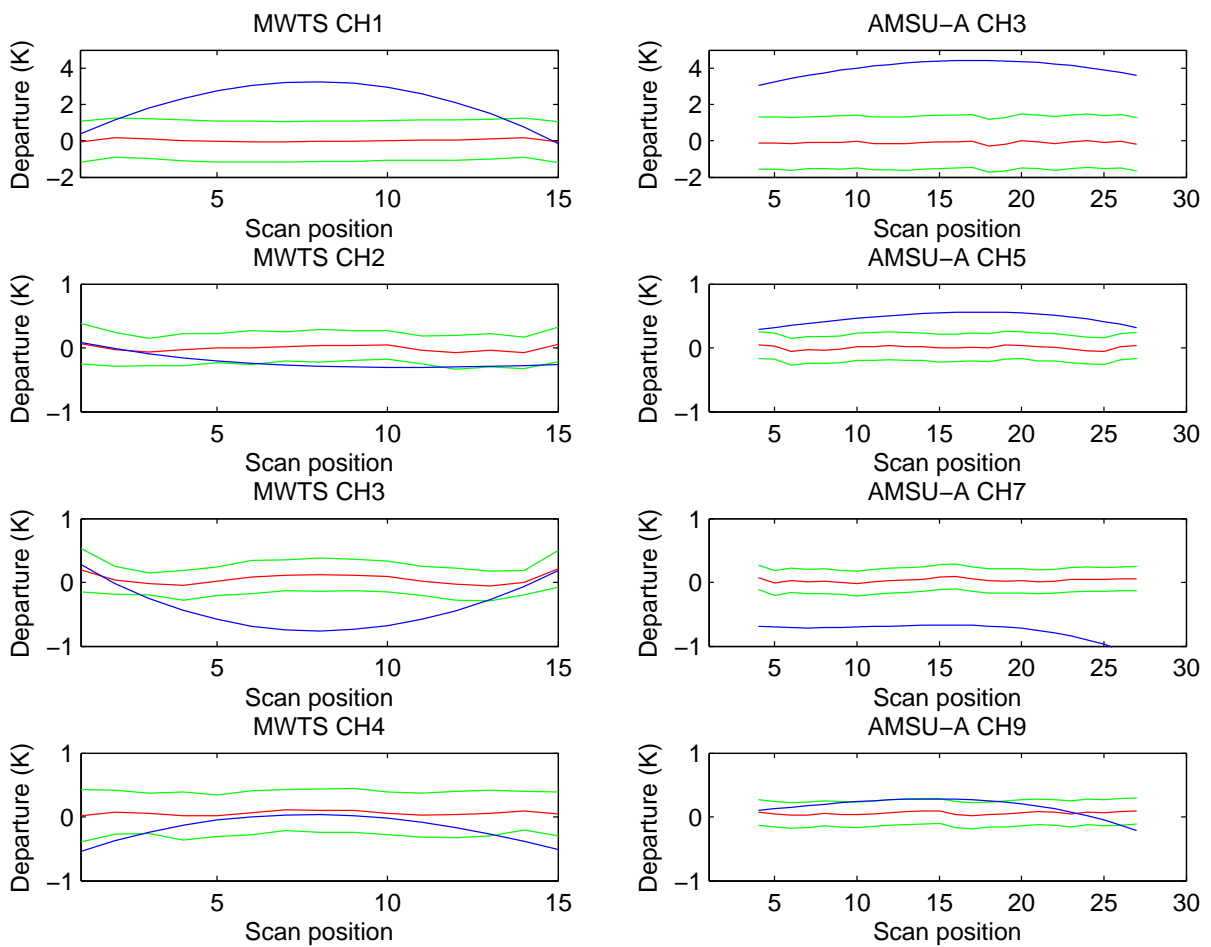
Figure 13: First guess departure statistics and bias correction versus scan position for FY-3A MWTS and equivalent MetOp-A AMSU-A channels. Statistics are based on 9 days of used data (20-28 September 2008). Red indicates the mean departure after bias correction, with the green lines indicating $\pm$ one standard deviation. Blue is the mean bias correction.
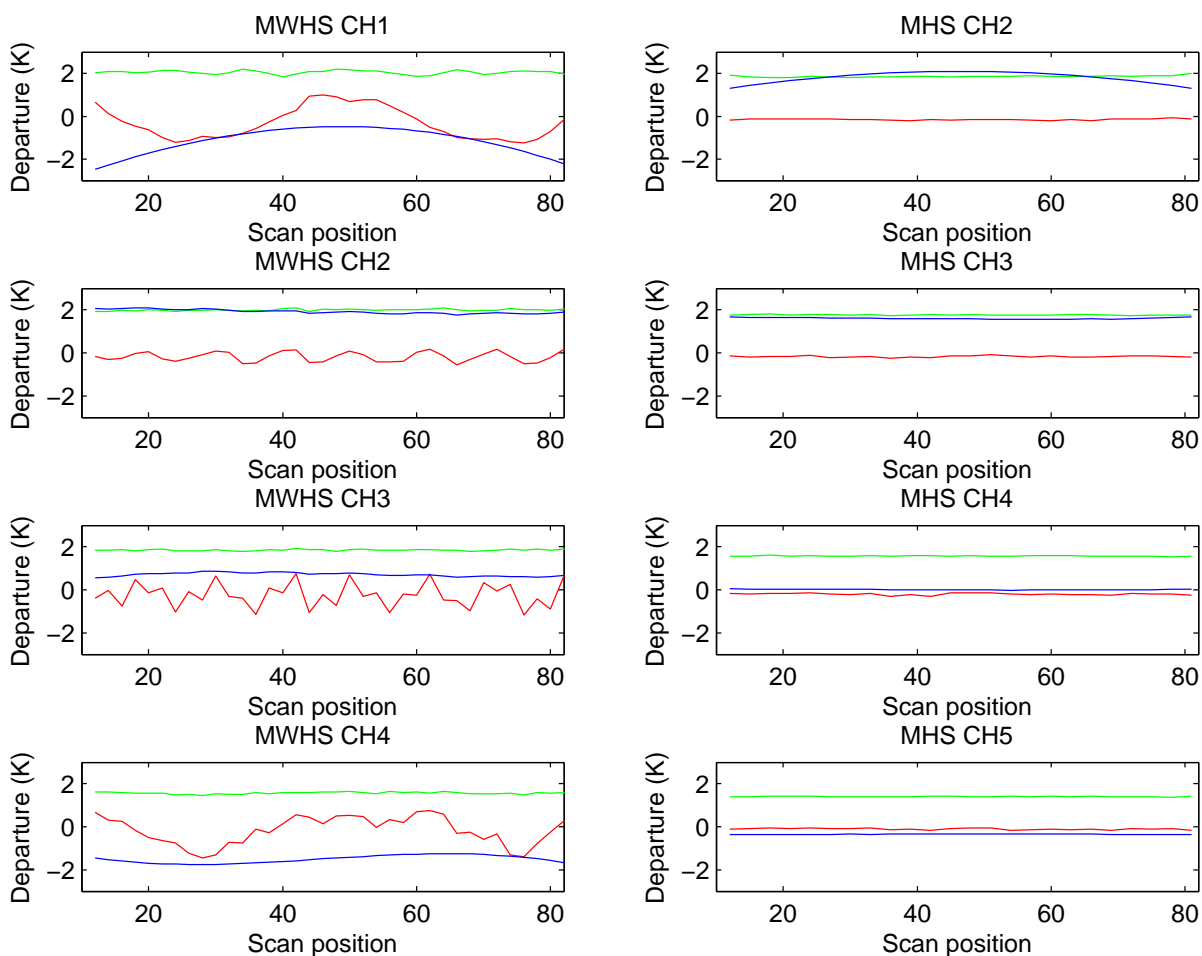
Figure 14: First guess departure statistics and bias correction versus scan position for FY-3A MWHS and equivalent MetOp-A MHS channels. Statistics are based on 9 days of used data (20-28 September 2008). Red indicates the mean departure after bias correction, with the green lines indicating the standard deviation. Blue is the mean bias correction.
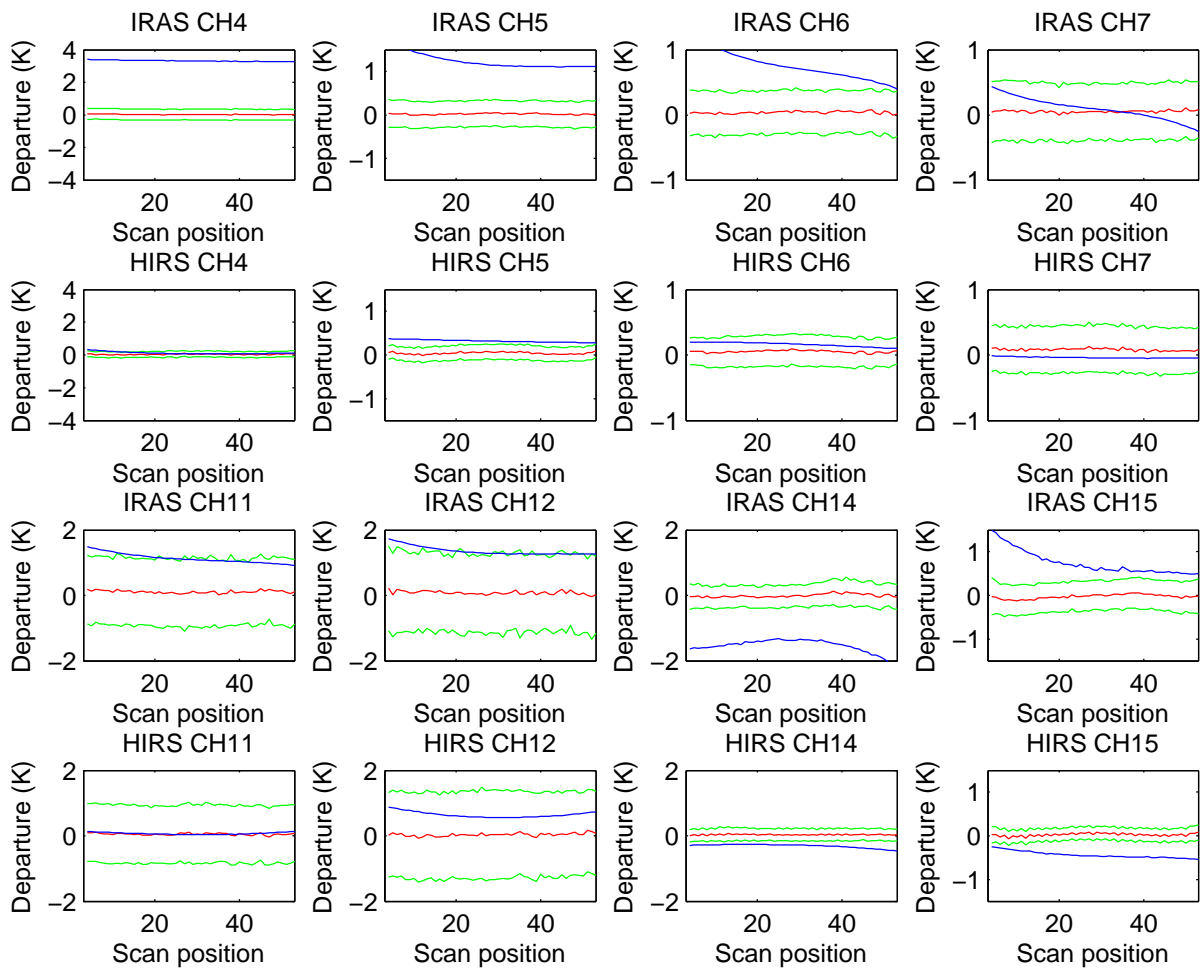
Figure 15: First guess departure statistics and bias correction versus scan position for FY-3A IRAS and equivalent MetOp-A HIRS channels. Statistics are based on 9 days of used data (20-28 September 2008). Red indicates the mean departure after bias correction, with the green lines indicating ± one standard deviation. Blue is the mean bias correction.
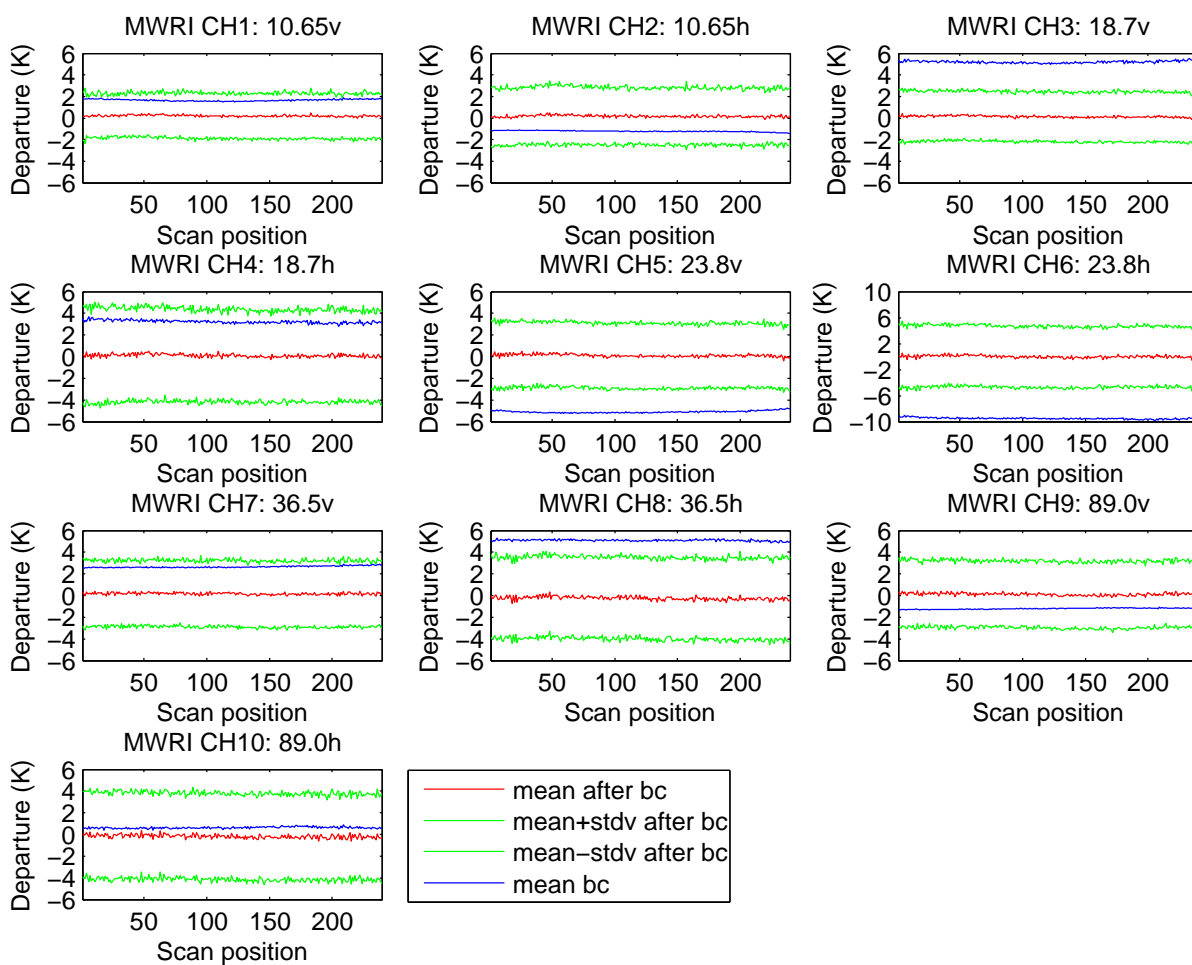
Figure 16: First guess departure statistics and bias correction versus scan position for FY-3A MWRI. Statistics are based on 8 days of used data (10-17 September 2008).
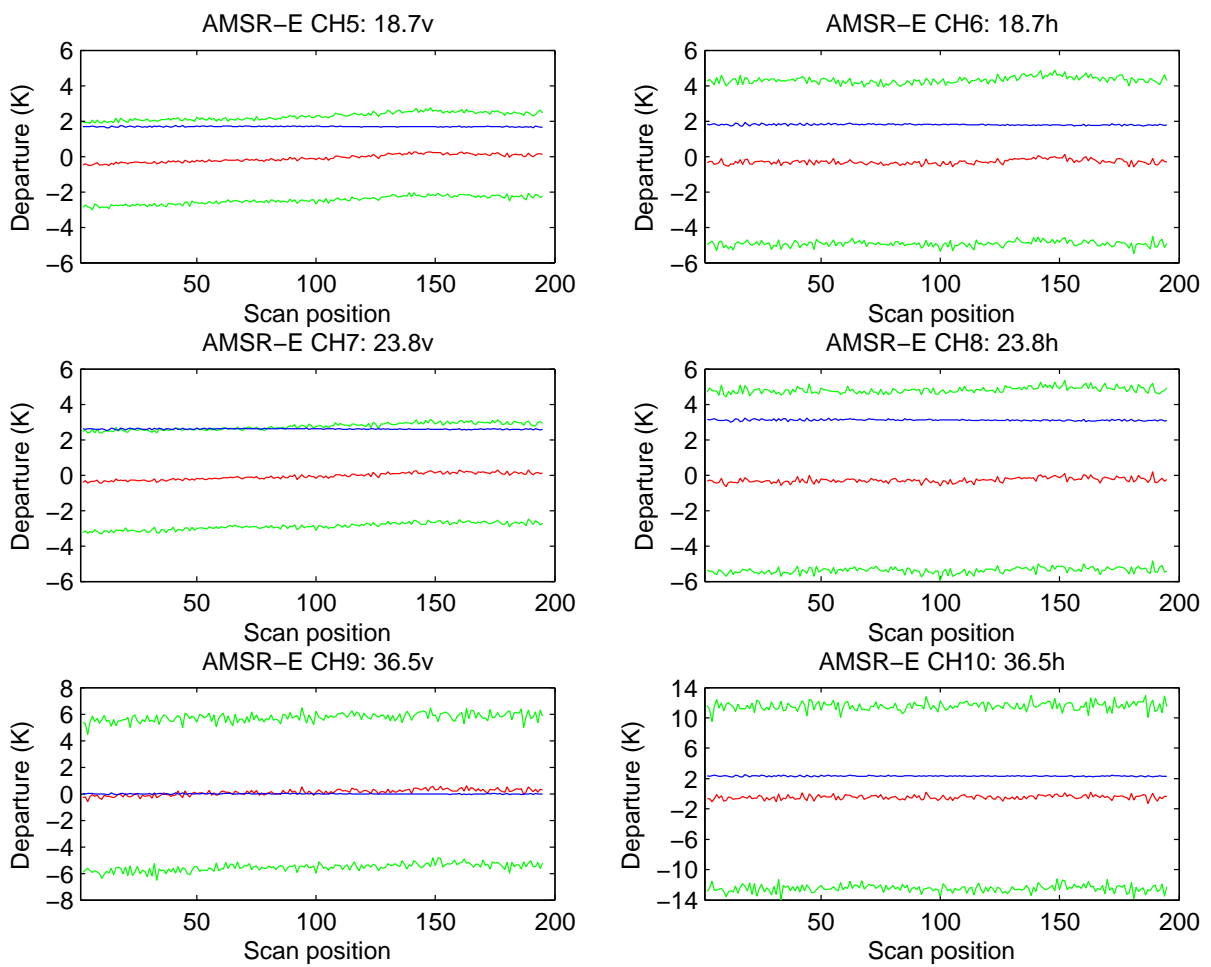
Figure 17: First guess departure statistics versus scan position for AQUA AMSR-E channels.
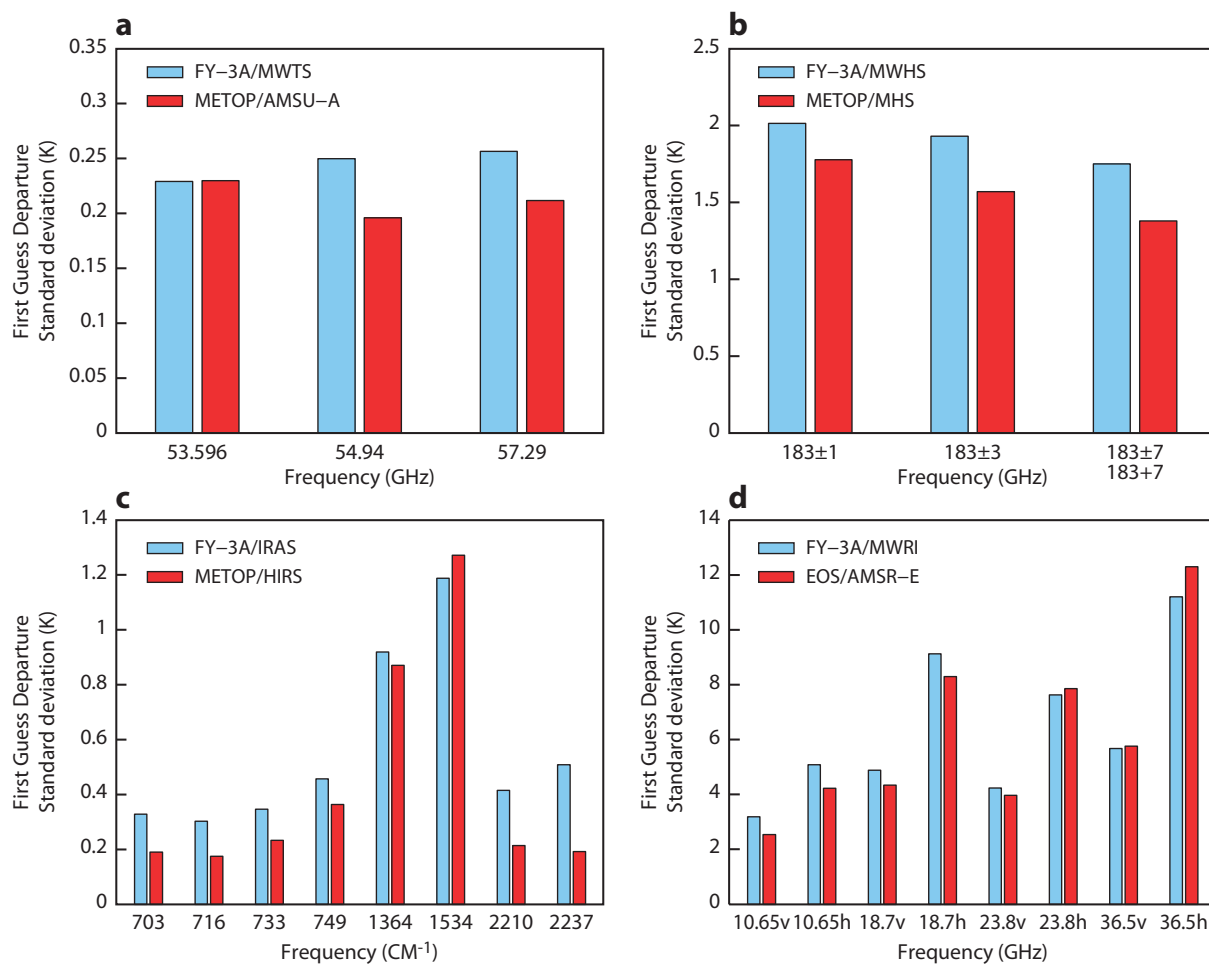
Figure 18: Standard deviations for FY-3A and METOP/AQUA equivalent instruments and channels. Statistics are derived from used data for the period from 28 August to 28 September 2008: a) MWTS and AMSU-A; b) MWHS and AMSU-B ; c) IRAS and HIRS ; d) MWRI and AMSR-E.
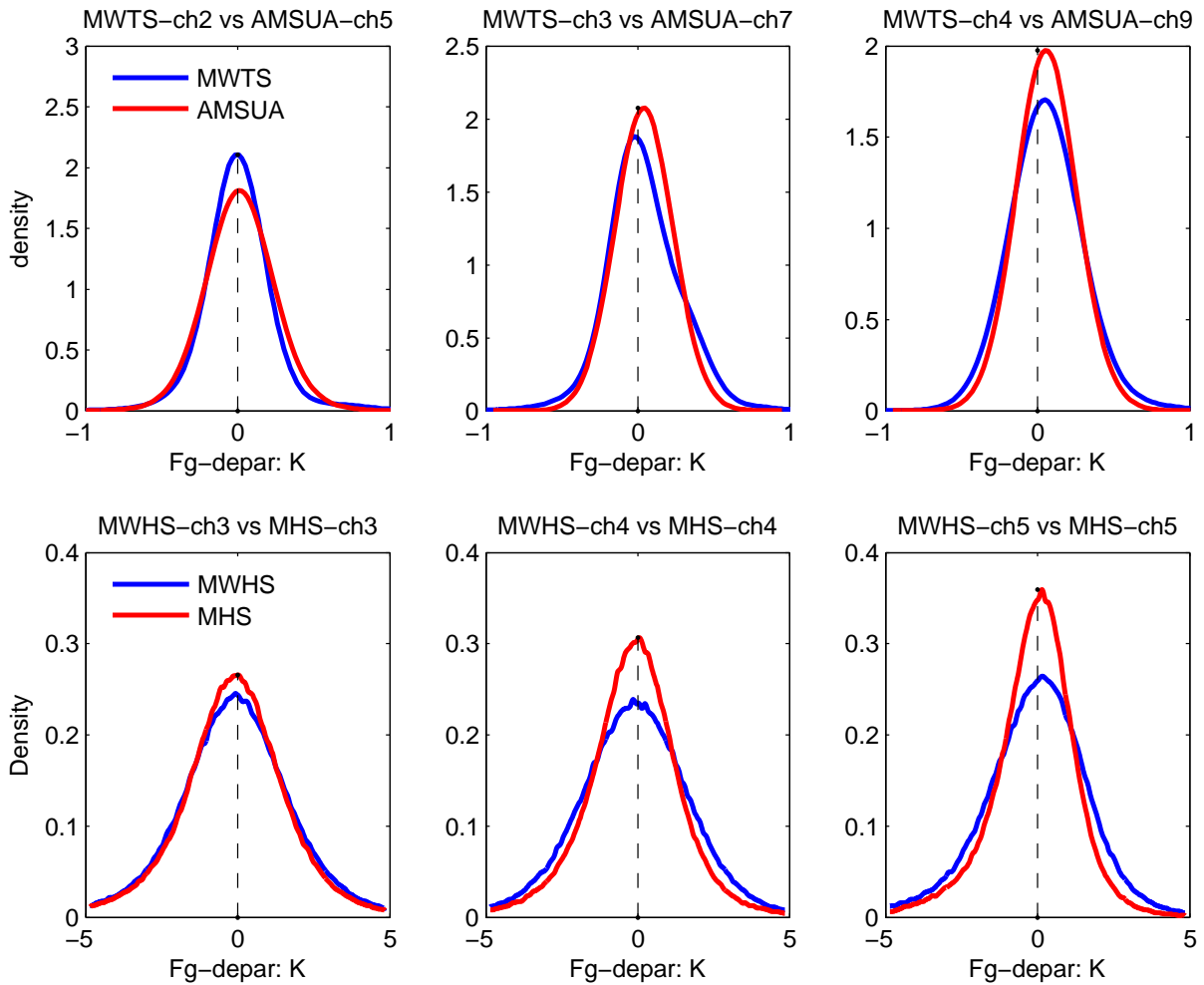
Figure 19: (Top row) Histograms of first guess departures for MWTS channels 2 (53.6 GHz), 3 (54.9 GHz) and 4 (57.3 GHz) and equivalent AMSU-A channels (channels 5, 7 and 9). (Bottom row) first guess departures for MWHS channels 3 (183±1 GHz), 4 (183±3 G Hz) and 5 (183±7 GHz) and equivalent MHS channels (channels 3, 4 and 5). Statistics were derived from used data for the period 28 August to 28 September 2008.
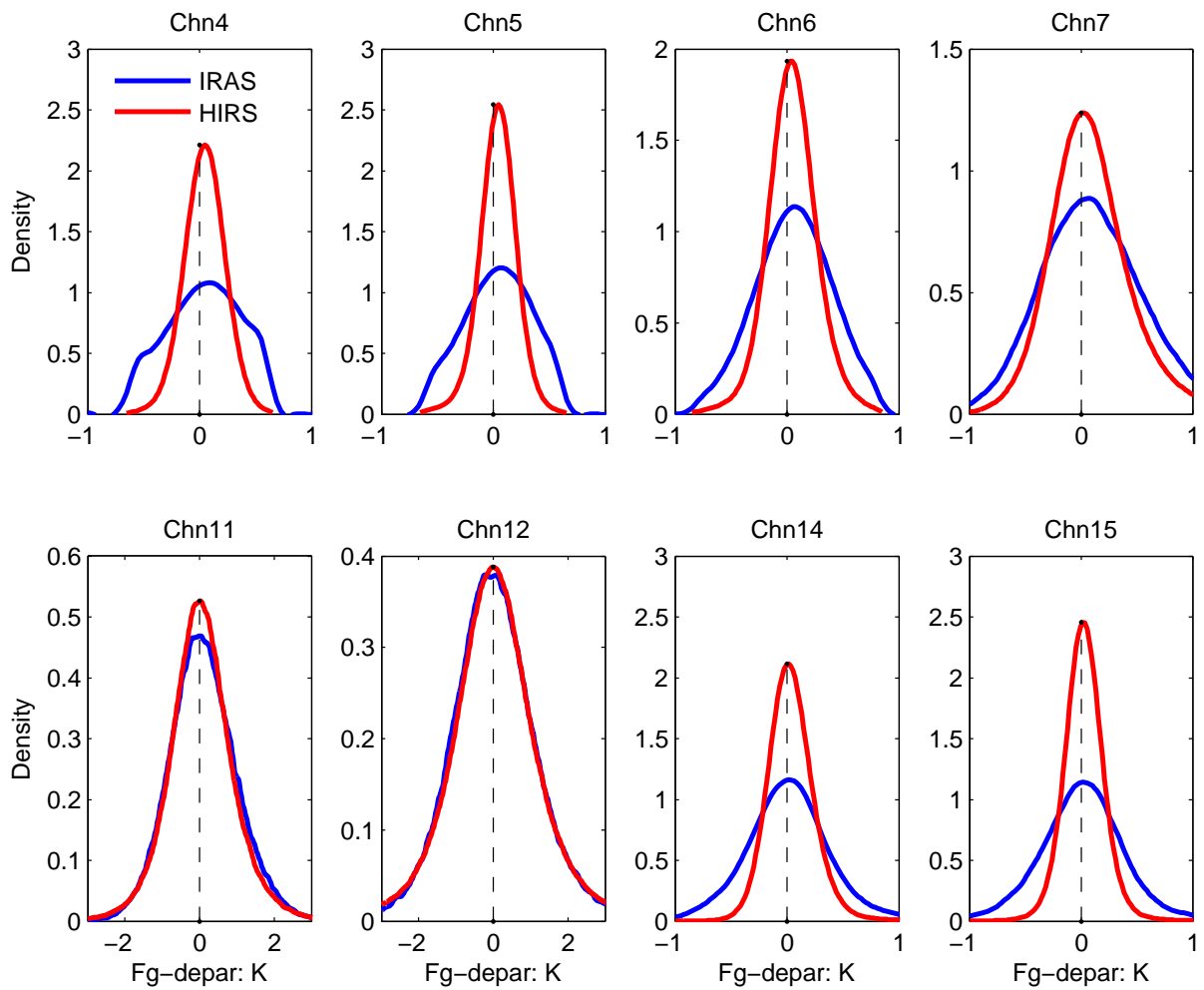
Figure 20: Histograms of first guess departures for IRAS channels (4-7,11-12,14-15) and equivalent HIRS channels. Statistics were derived from used data for the period 28 August to 28 September 2008.
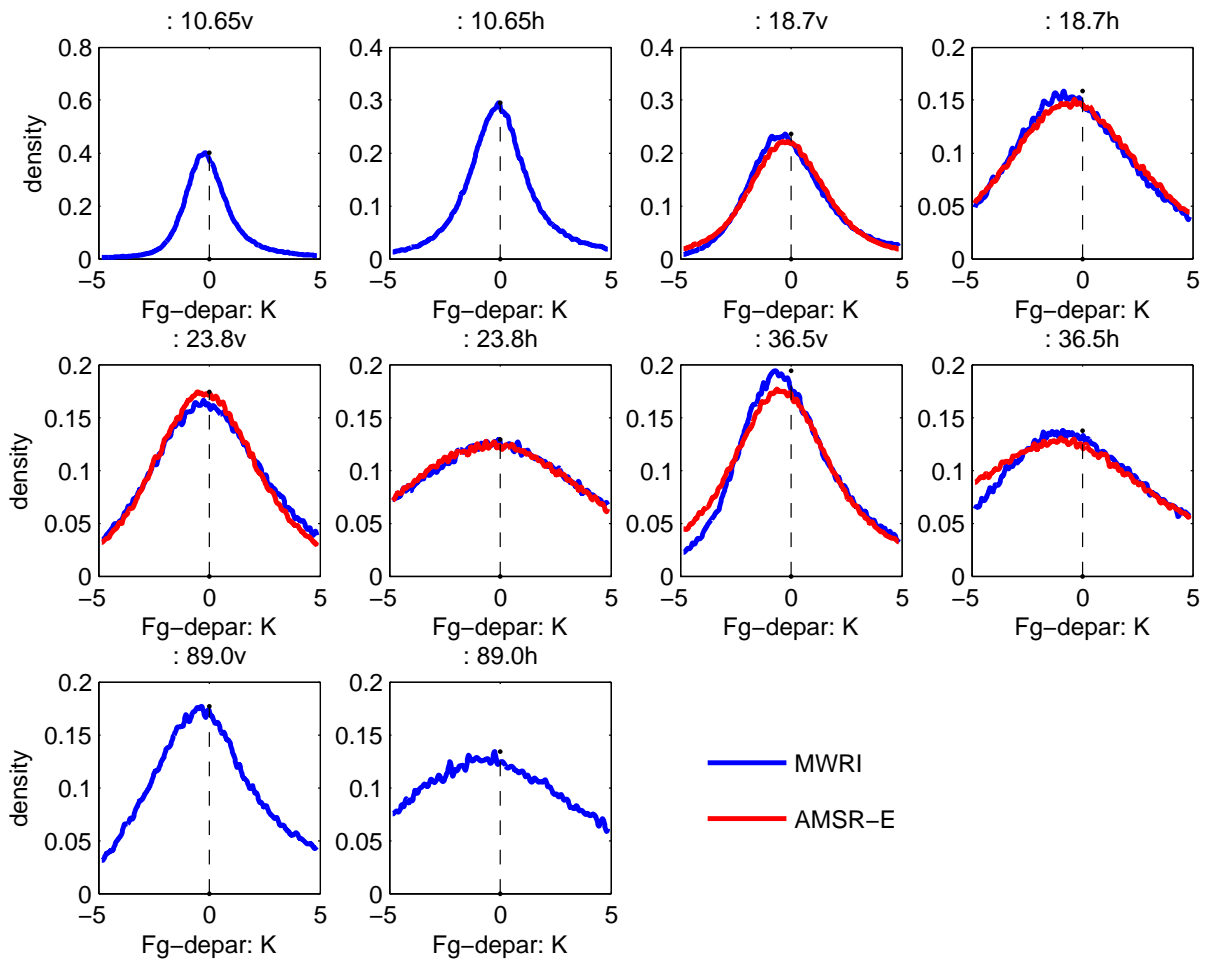
Figure 21: Histograms of first guess departures for MWRI channels and equivalent AMSR-E channels (where available). Statistics were derived from used data for the period 10 to 17 September 2008.
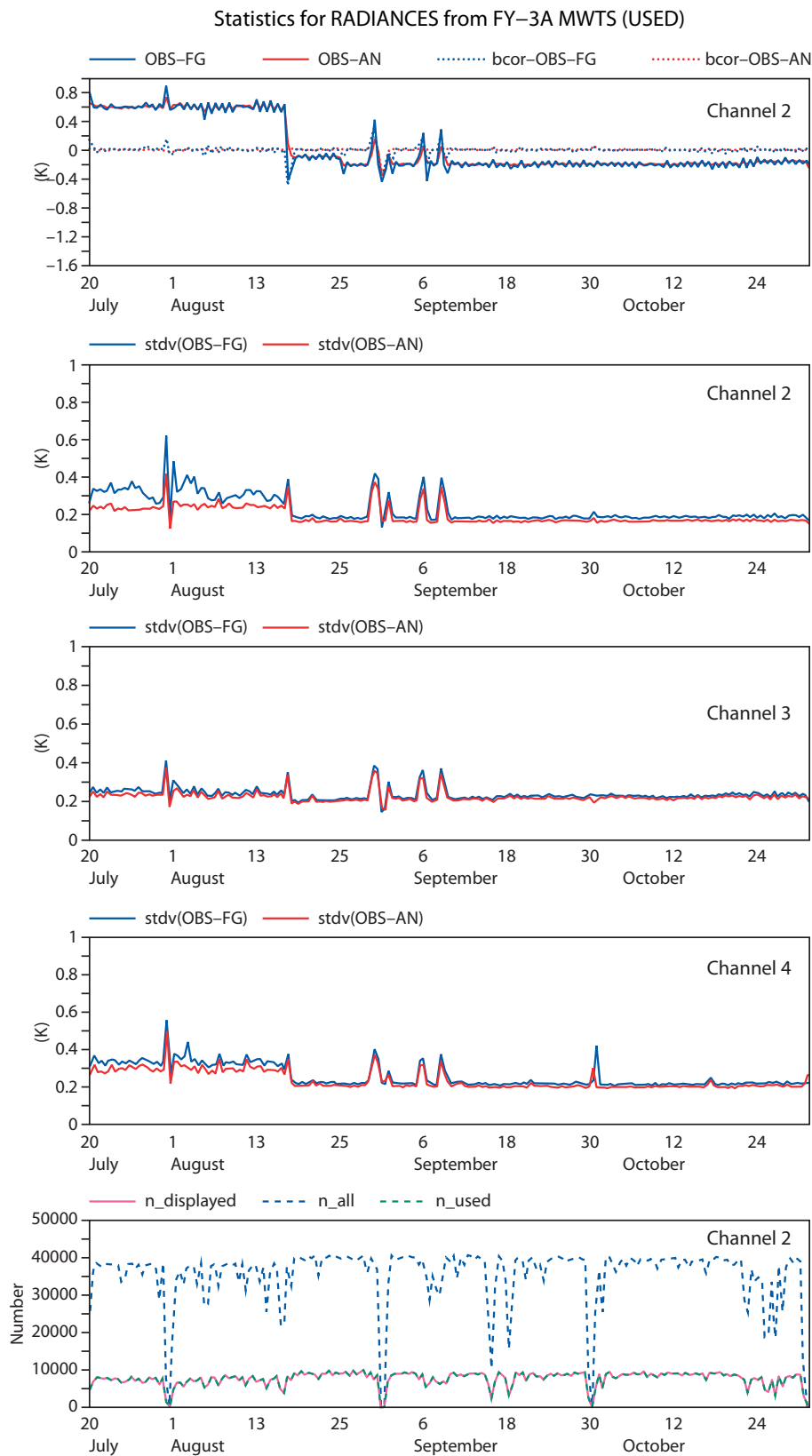
Figure 22: Time series of mean (channel 2 only) and standard deviations of the first guess and analysis departures for MWTS channels 2-4. Also shown (bottom plot, channel 2 only) are the observation numbers during this period.
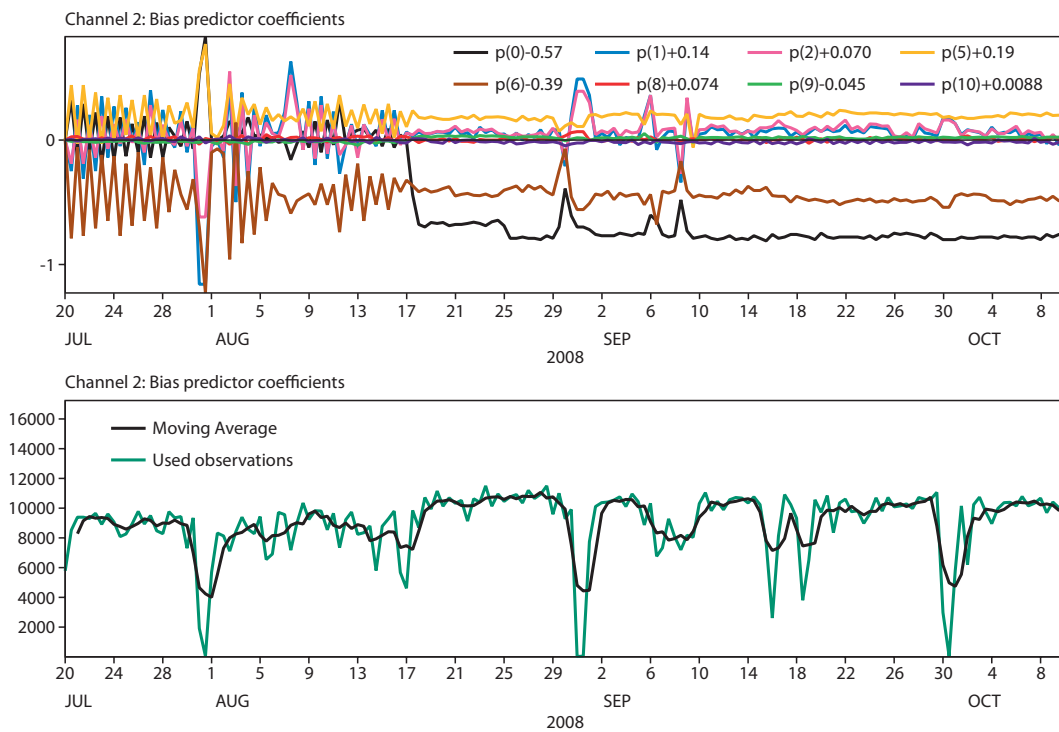
Figure 23: Bias correction coefficient evolution for MWTS.
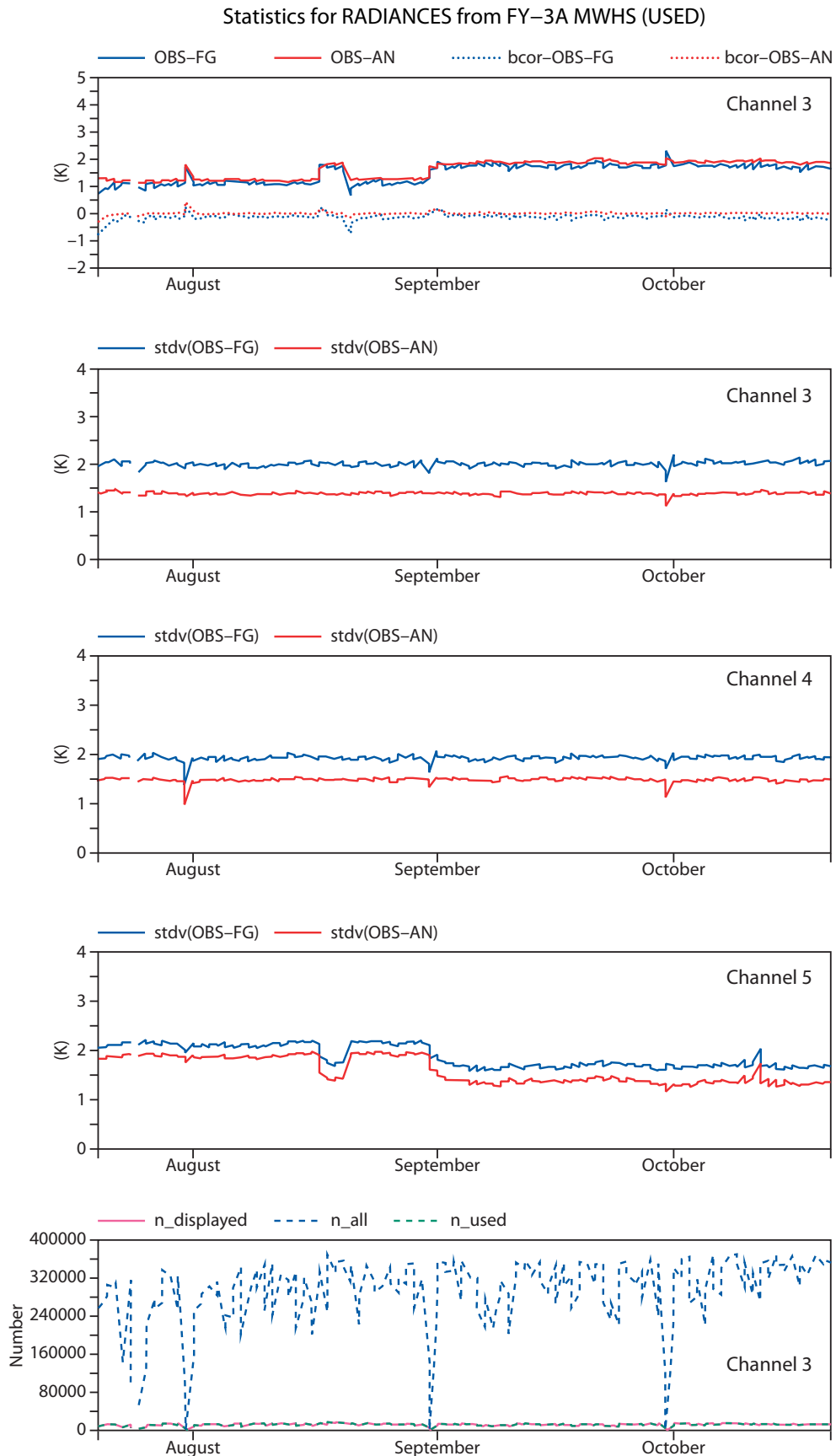
Figure 24: Time series of mean (channel 3 only) and standard deviations of the first guess and analysis departures for MWHS channels 3-5. Also shown (bottom plot, channel 3 only) are the observation numbers during this period.
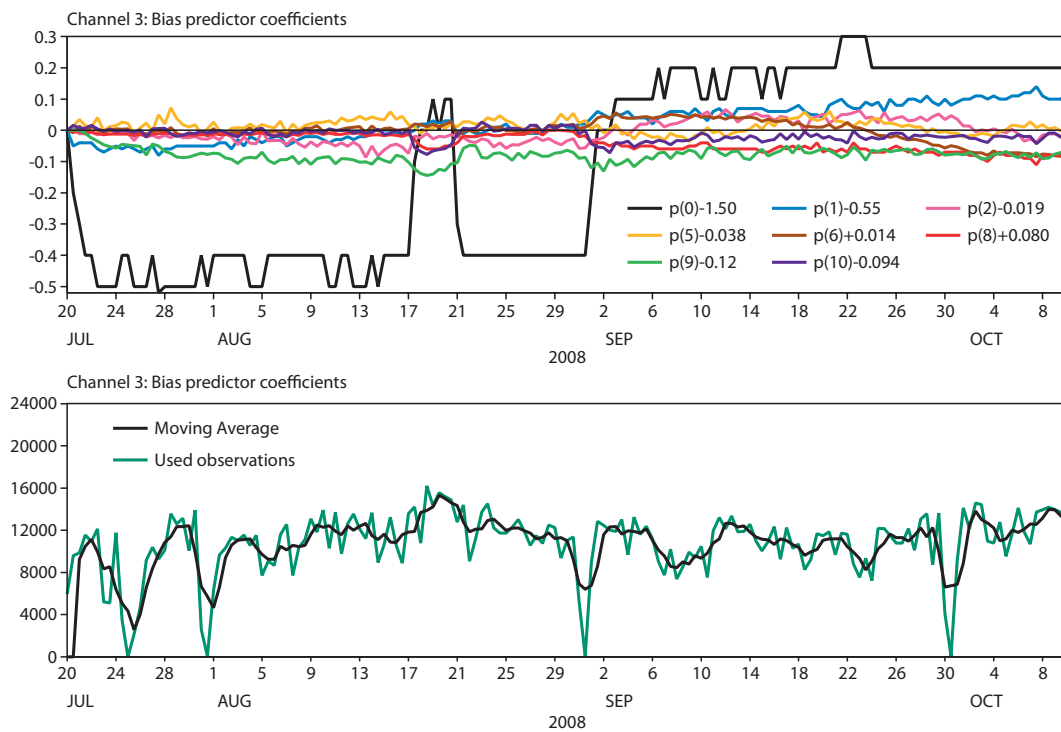
Figure 25: Bias correction coefficient evolution for MWHS.

Statistics for RADIANCES from FY−3A IRAS (USED)
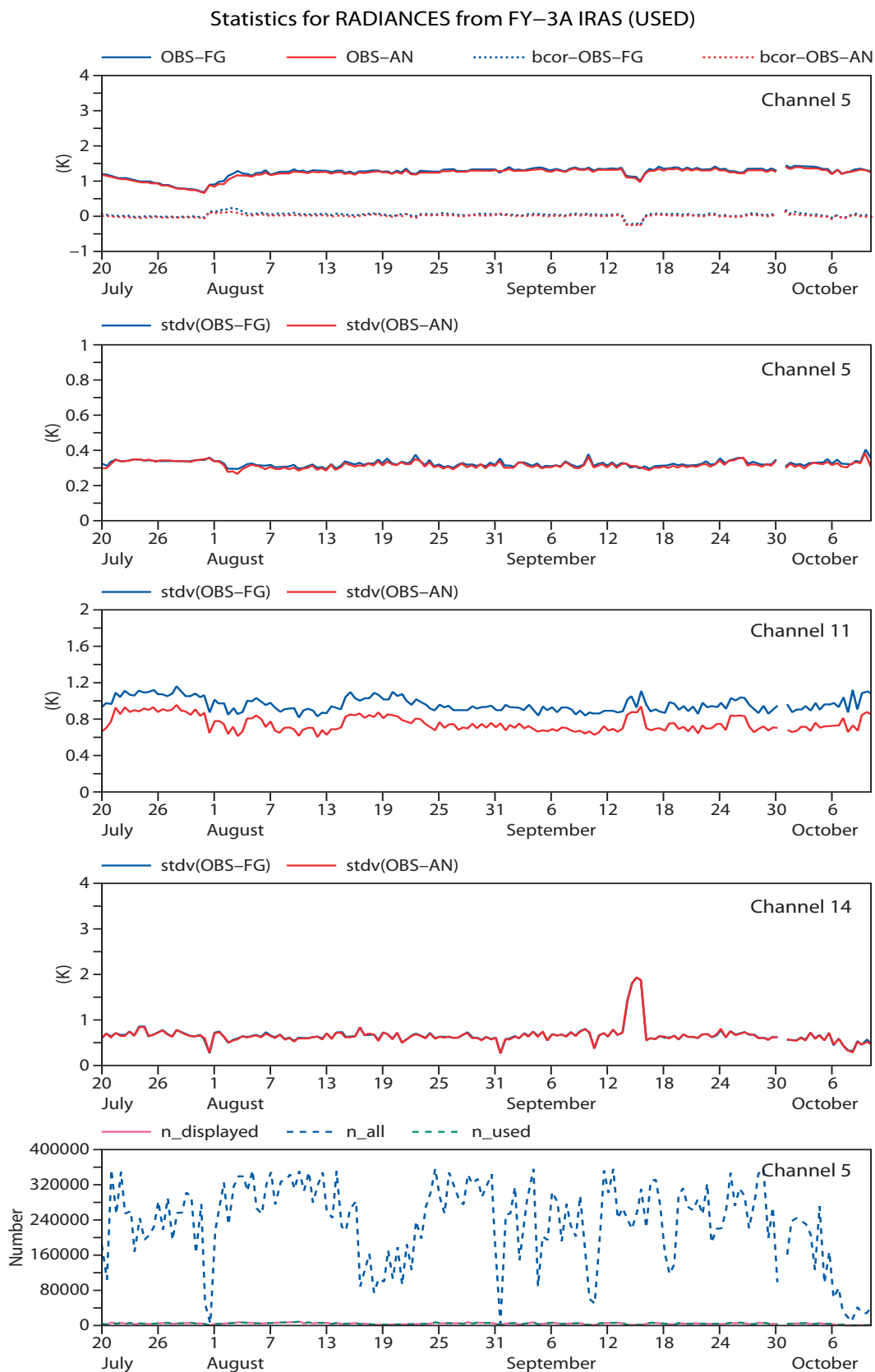
Figure 26: Time series of mean (channel 5 only) and standard deviations of the first guess and analysis departures for IRAS channels 5, 11 and 14. Also shown (bottom plot, channel 5 only) are the observation numbers during this period. This subset of channels were selected to be representative of the temperature (channel 5), water vapour (channel 11) and short wave temperature sounding channels (14).
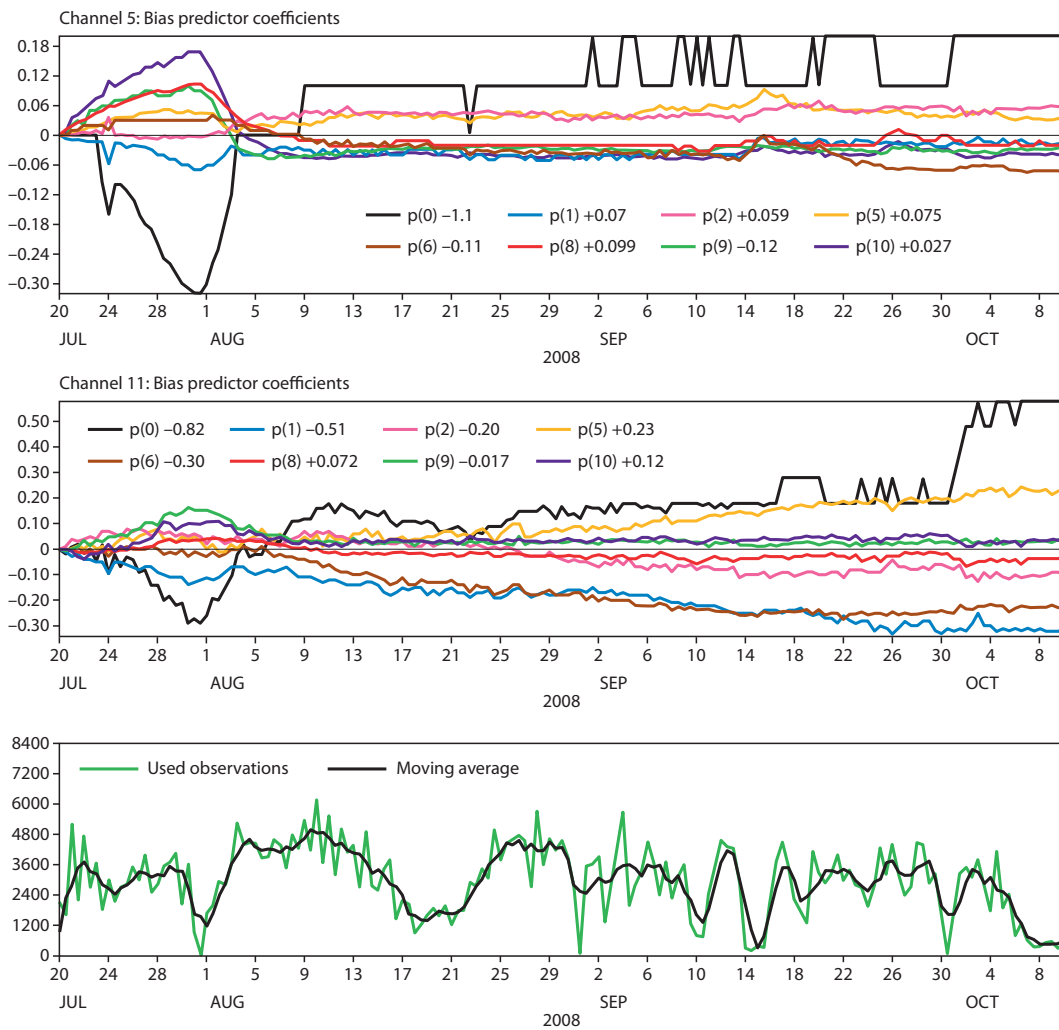
Figure 27: Bias correction coefficient evolution for IRAS.
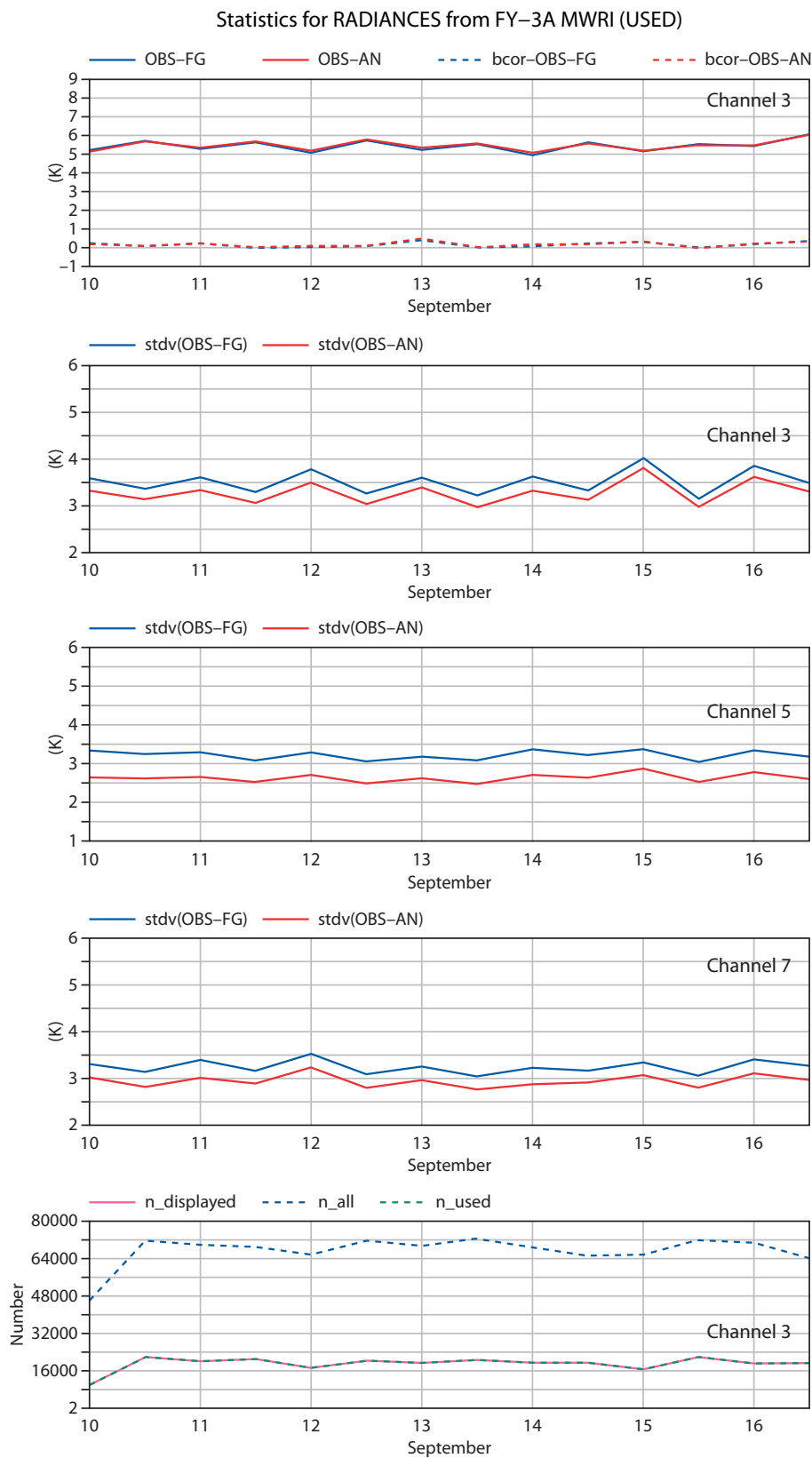
Figure 28: Time series of mean (channel 3 only) and standard deviations of the first guess and analysis departures for MWRI channels 3, 5 and 7. Also shown (bottom plot, channel 3 only) are the observation numbers during this period.
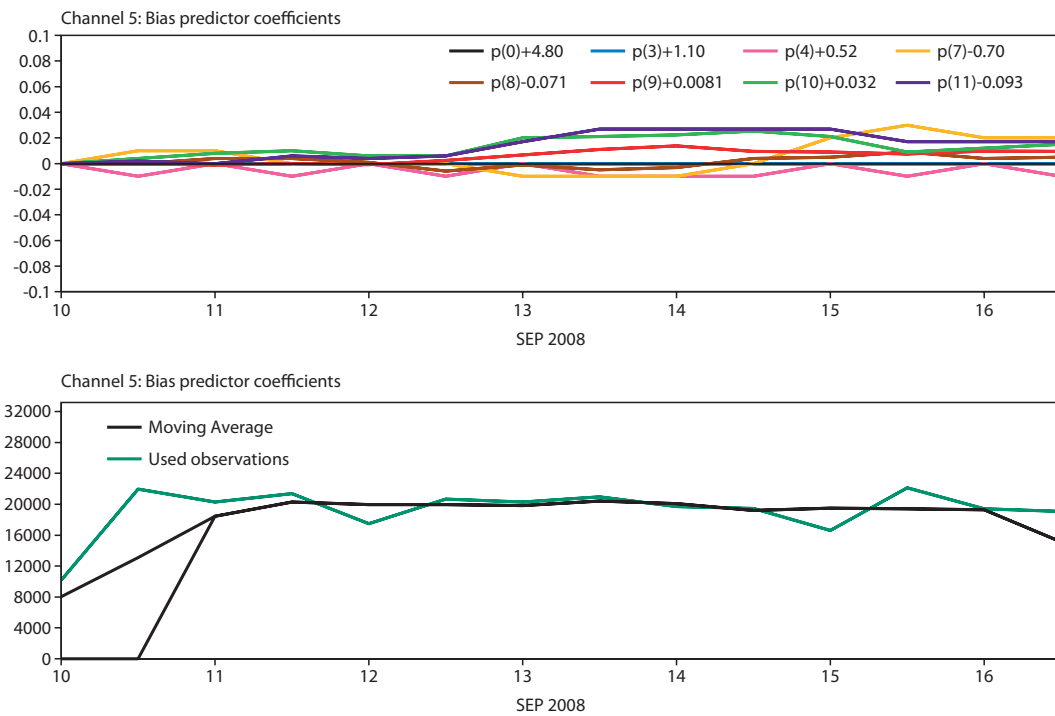
Figure 29: Bias correction coefficient evolution for MWRI
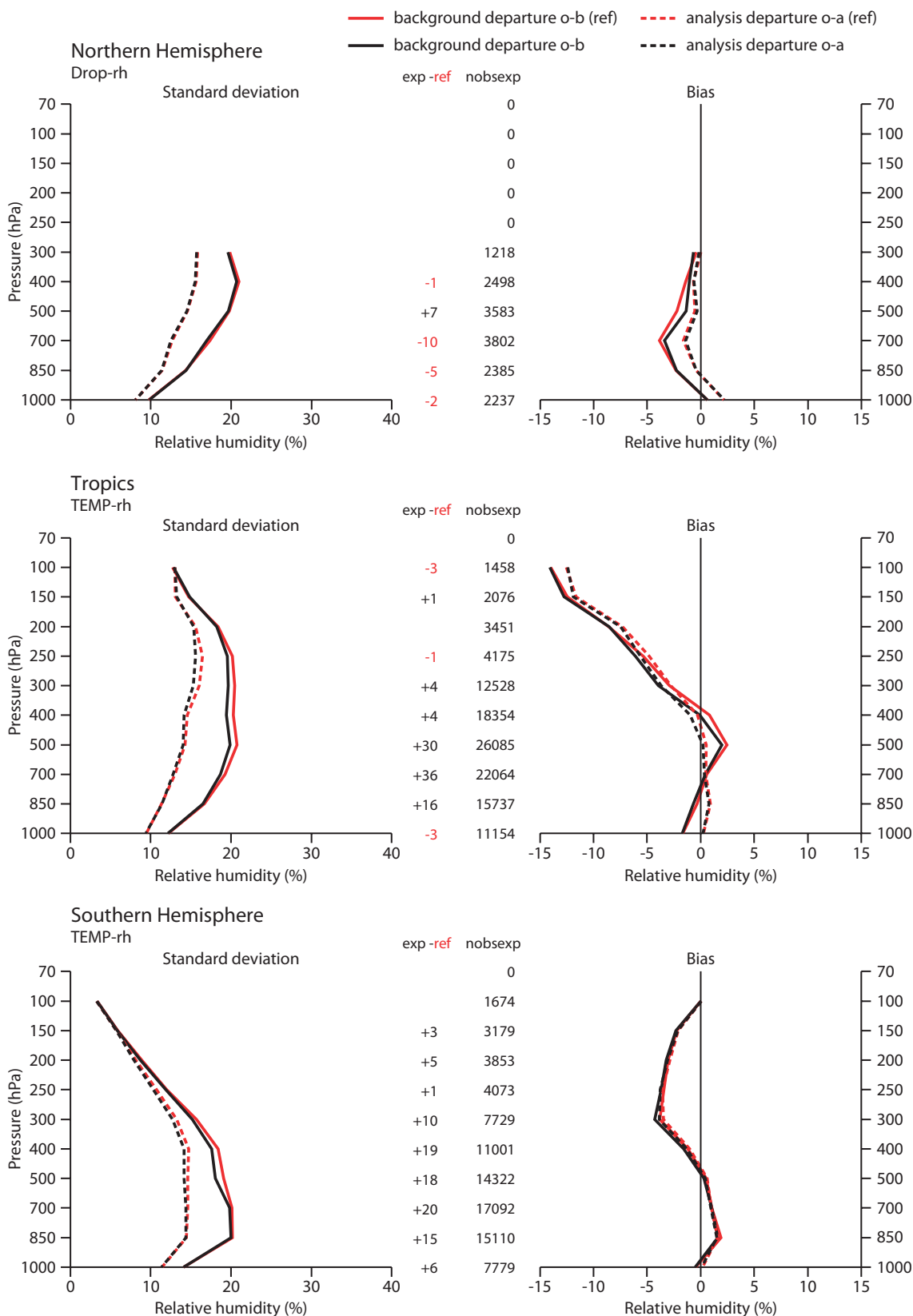
Figure 30: First guess and analysis departure statistics for relative humidity from dropsondes in the NH (top) and radiosondes in the Tropics (middle) and SH (bottom). in %, for 28 August to 28 September 2008. Baseline + FY3A MWHS is in black and the Baseline experiment is in red.
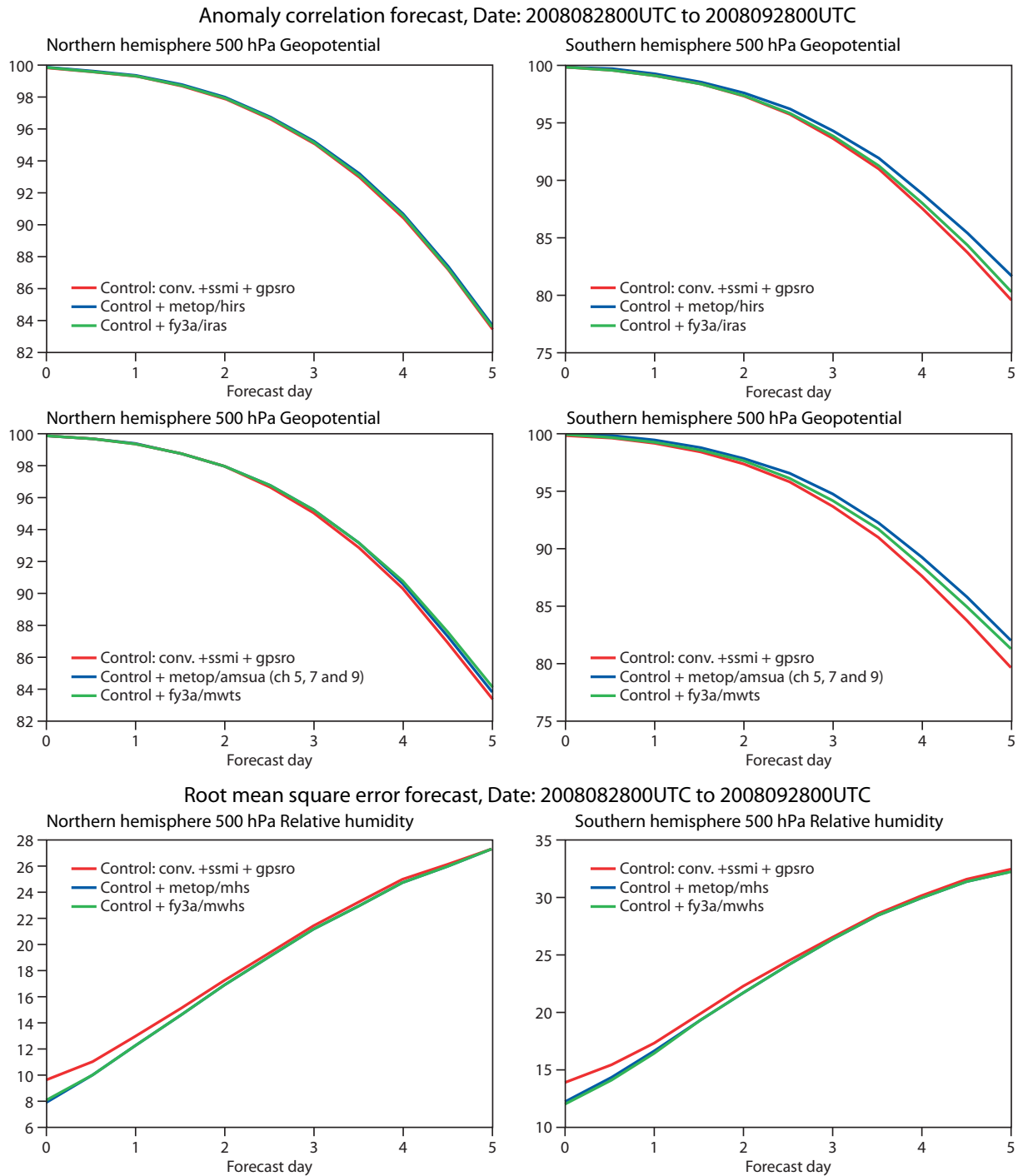
Figure 31: *Anomaly correlation for 500 hPa geopotential height (in the top and middle row) and Root mean square error for 500 hPa relative humidity (in the bottom row) in the northern hemisphere (left) and the southern hemisphere (right) for an observing system depleted control experiment (red) as well as experiments in which either FY-3A (green) or MetOp-A (blue) sounding data has been added.*
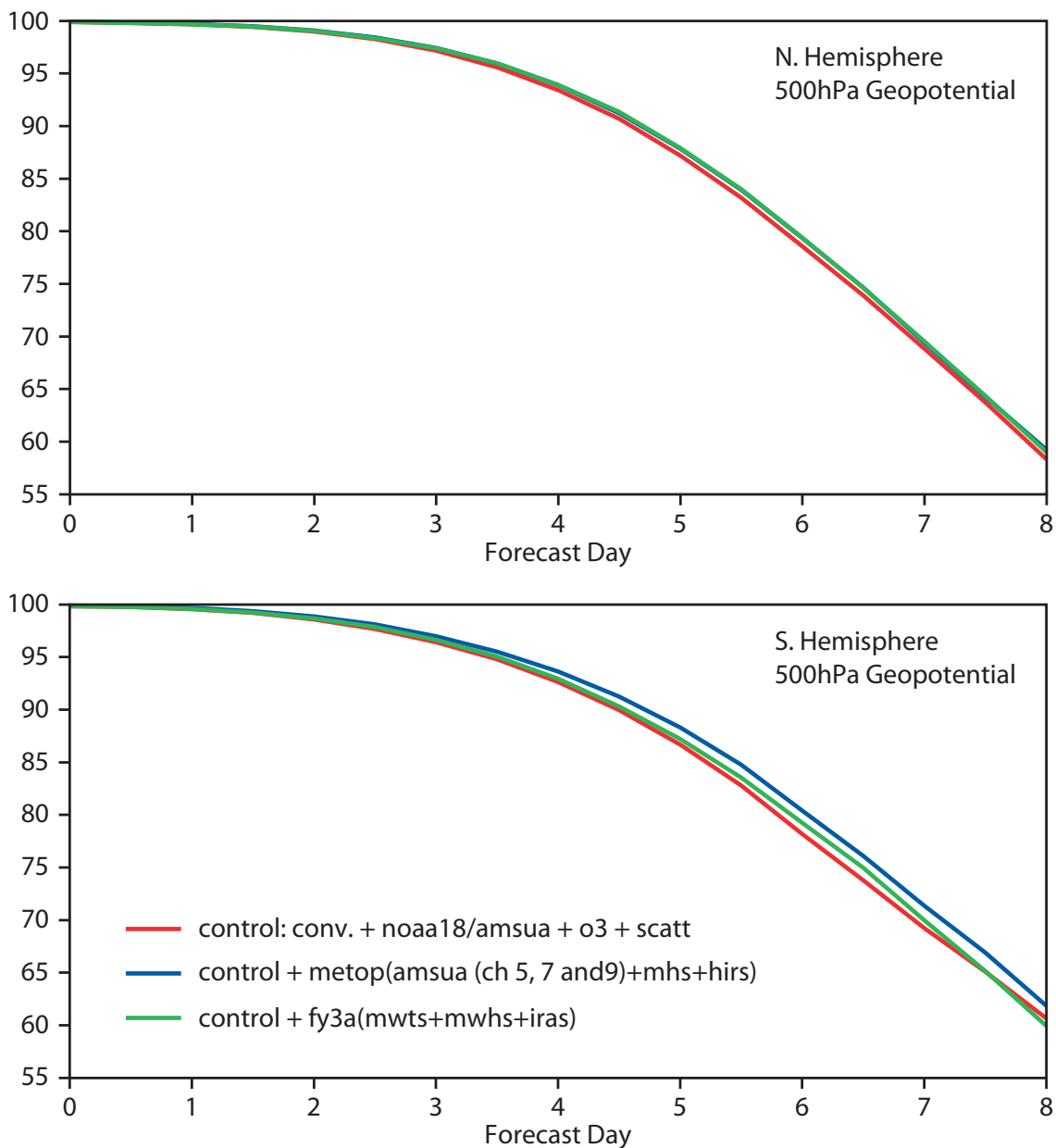
Figure 32: Anomaly correlation for 500 hPa geopotential height in the northern hemisphere (top) and the southern hemisphere (bottom) for an observing system depleted control experiment (red) as well as experiments in which either FY-3A (green) or MetOp-A (blue) sounding data has been added.
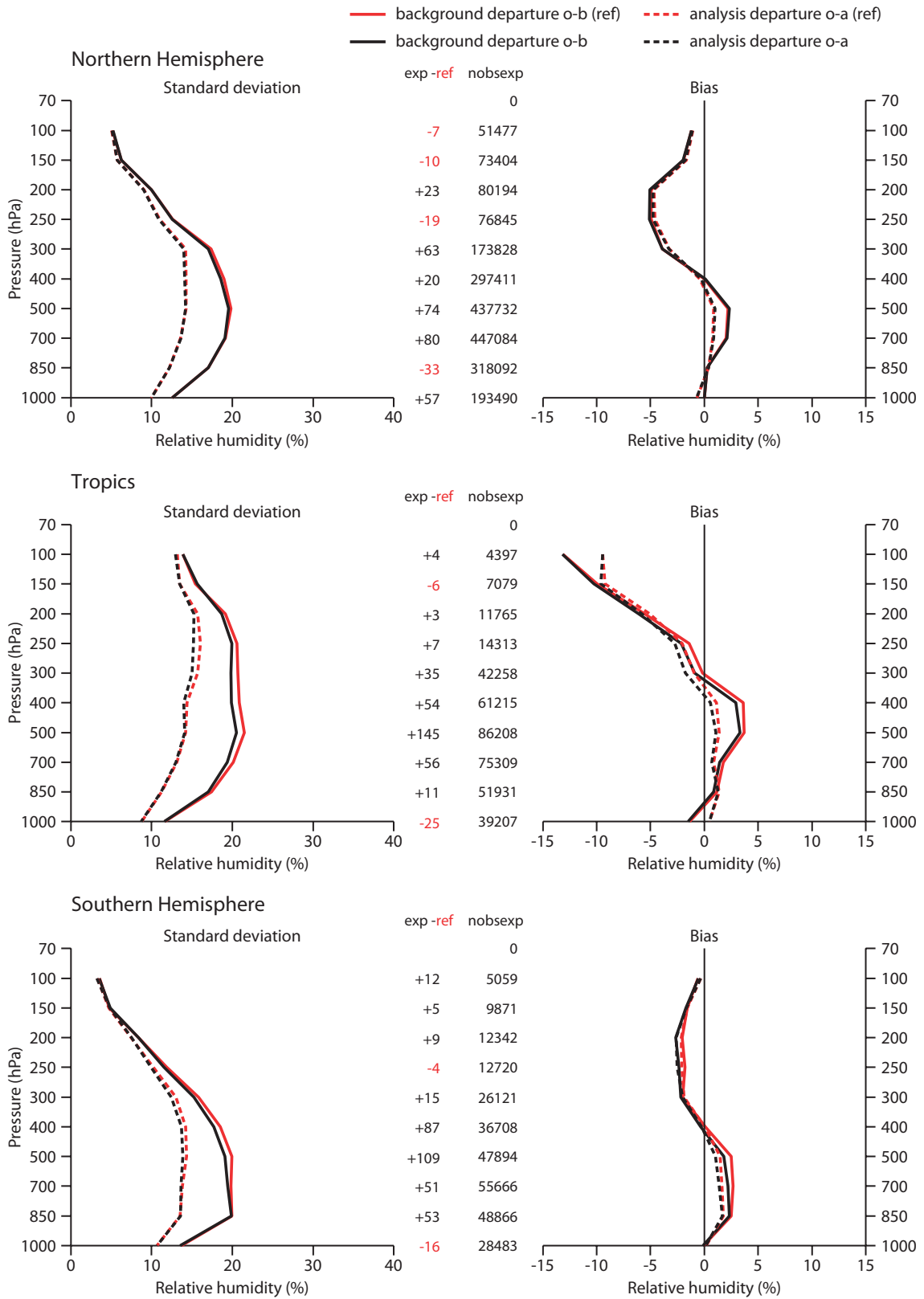
Figure 33: First guess and analysis departure statistics for radiosonde humidity in the NH (top), Tropical(middle) and SH (bottom) for 20 July to 30 October 2008. Baseline experiment + FY3A VASS is in black and the baseline experiment is in red.
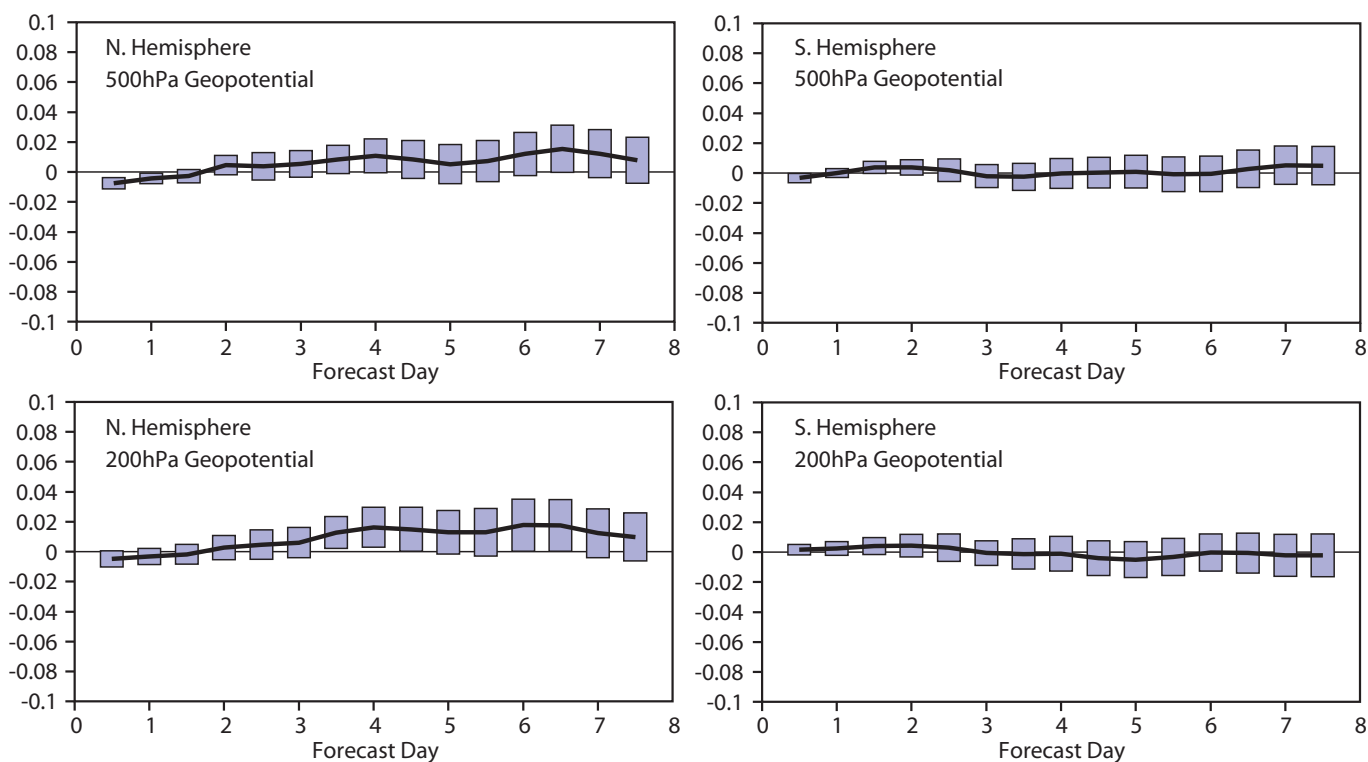
Figure 34: Normalised differences in the root mean squared forecast error between the Full + FY3A experiment and the Full system experiment ((Full system minus Full system + FY-3A), i.e. up indicates a positive benefit from FY-3A data*) for the 00 Z forecast of the 500 hPa geopotential height for the NH (left) and the SH (right). Verification is against operations, and the period is 10 August - 1 November 2008 (93 cases), the experiments were run from 20 July to 1 November 2008. Error bars indicate 90 % significance intervals from a t−test.*

RMS forecast errors (Experiment–Control), 30–Jul–2008 to 30–Oct–2008, from 86 to 93 samples.
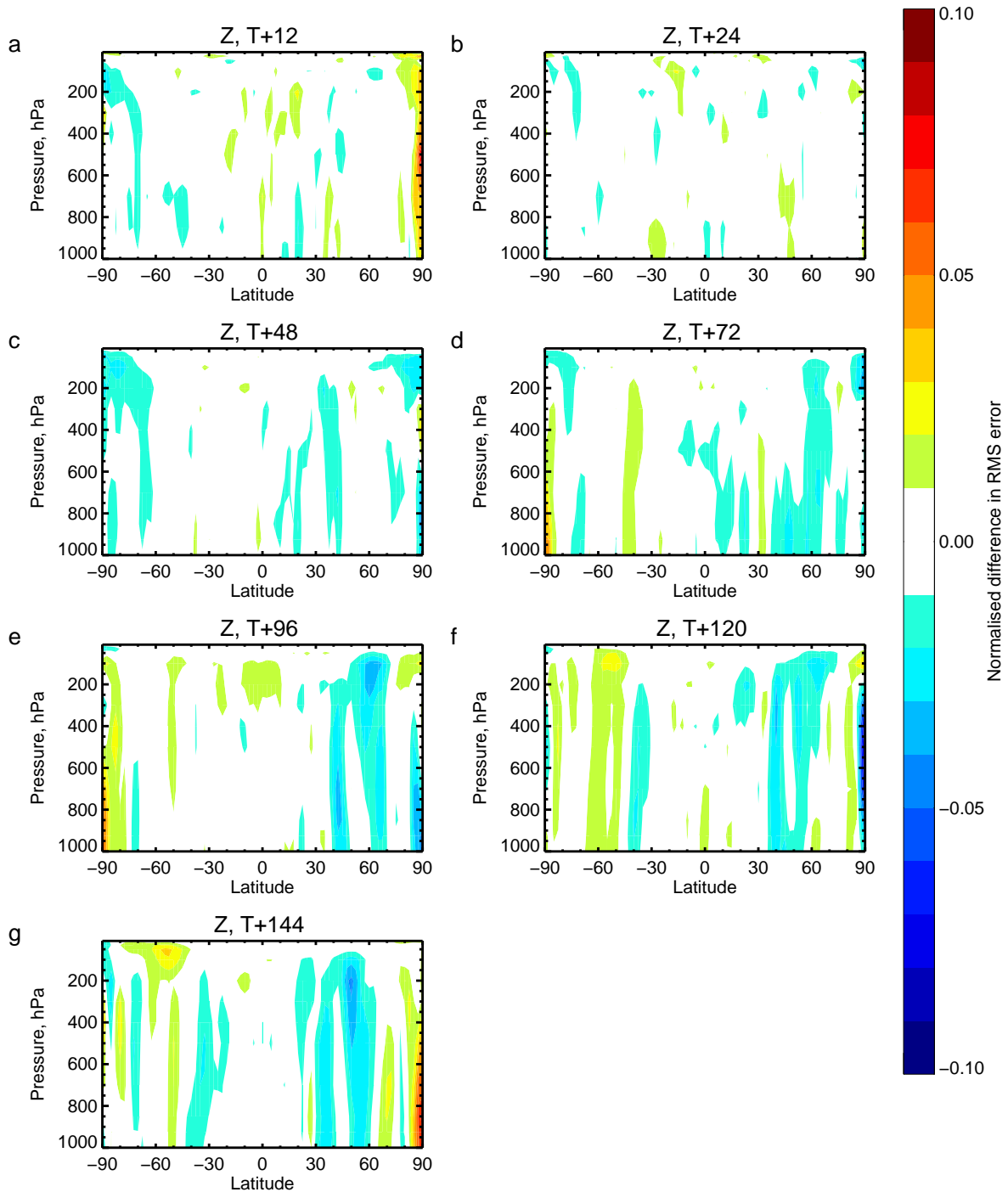
Figure 35: *Zonal means of normalised differences in the root mean square forecast error for geopotential height between the Full + FY3A and the control Full experiment. Blue shading indicates an improvement in the Full + FY3A experiment compared to the control. Forecasts are verified against own analyses from the respective experiment. Scores are shown for the period 30 July - 30 October 2008 (86-93 samples, depending on forecast range). Each panel shows the differences for the forecast range indicated above the panel.*
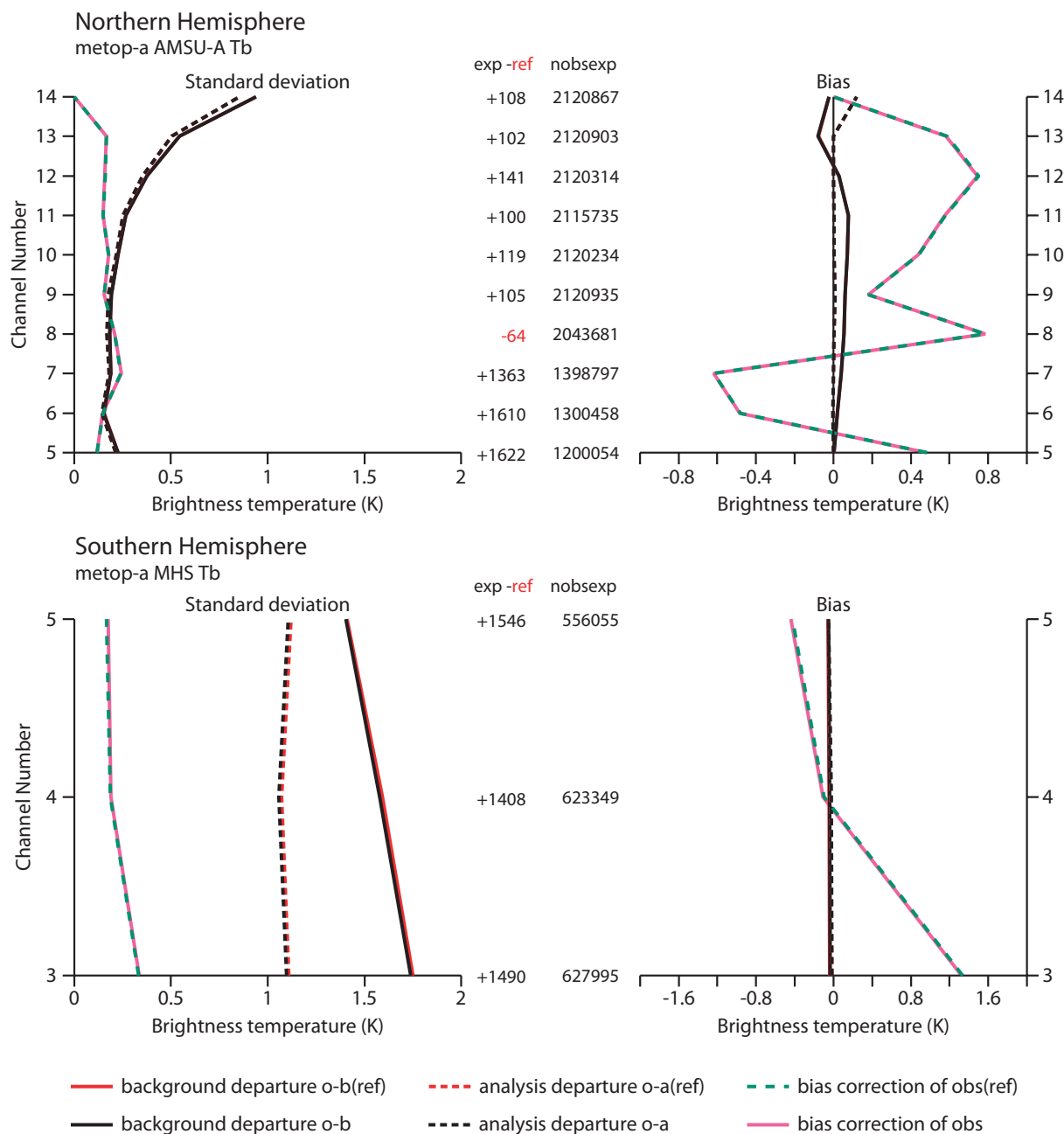
Figure 36: First guess and analysis departure statistics for NH METOP-A AMSU-A and SH METOP-A MHS FG departures, in K, for 20 July to 30 October 2008. Full + FY3A VASS is in black and Control Full is in red.

Table 1: FY-3A MWTS, and equivalent AMSU-A, channel characteristics and assumed observation errors (R).

Channel number	Frequency / GHz	Bandwidth / MHz	MWTS NEΔT (pre-launch) / K	Equiv AMSU-A channel number	AMSU-A NEΔT / K	R MWTS / K	R ((AMSU-A) / K
1	50.3	180	0.5	3	0.40	–	–
2	53.596± 0.115	2×170	0.4	5	0.25	0.43	0.35
3	54.94	400	0.4	7	0.25	0.52	0.35
4	57.29	330	0.4	9	0.25	0.55	0.35

Table 2: FY-3A MWHS channel characteristics and assumed observation errors (R).

Channel number	Frequency / GHz (pol)	Bandwidth / MHz	MWHS NEΔT / K	MHS Channel number	MHS NEΔT / K	R MWHS / K	R MHS / K
1	150(v)	1000	0.9	2	0.84	–	–
2	150(h)	1000	0.9				
3	183.31±1	500	1.1	3	0.60	2.26	2.0
4	183.31±3	1000	0.9	4	0.70	2.46	2.0
5	183.31±7	2000	0.9	5	1.06	2.39	2.0

Table 3: FY-3A IRAS channel characteristics and assumed observation errors (R).

Channel number	Frequency / cm^{-1}	Bandwidth / cm^{-1}	NEΔN (IRAS) mW m^{-2} sr^{-1} cm	HIRS Channel number	NEΔN (HIRS) mW m^{-2} sr^{-1} cm	R (IRAS) / K	R (HIRS) / K
1	669	3	4.00	1	3.00	–	–
2	680	10	0.80	2	0.67	–	–
3	690	12	0.60	3	0.50	–	–
4	703	16	0.35	4	0.31	1.10	0.60
5	716	16	0.32	5	0.21	0.99	0.60
6	733	16	0.36	6	0.24	0.80	0.60
7	749	16	0.30	7	0.20	0.83	0.75
8	802	30	0.20	8	0.15	–	–
9	900	35	0.15	9	0.10	–	–
10	1030	25	0.20	10	0.15	–	–
11	1345	50	0.23	11	0.20	0.90	0.91
12	1365	40	0.30	12	0.20	1.14	1.22
13	1533	55	0.30	13	0.006	0.80	0.50
14	2188	23	0.01	14	0.003	1.20	0.60
15	2210	23	0.01	15	0.004	–	–
16	2235	23	0.01	16	0.004	–	–
17	2245	23	0.01	17	0.002	–	–
18	2388	25	0.01	18	0.002	–	–
19	2515	35	0.01	19	0.001	–	–
20	2660	100	0.002				

Table 4: FY-3A MWRI channel characteristics.

Channel number (v,h) pairs	Frequency / GHz	Bandwidth / MHz	NEΔT (MWRI) / K	AMSR-E Channel number	Bandwidth / MHz	NEΔT (AMSR-E) / K
1,2	10.65	180	0.5	3,4	100	0.6
3,4	18.7	200	0.5	5,6	200	0.6
5,6	23.8	400	0.8	7,8	400	0.6
7,8	36.5	900	0.5	9,10	1000	0.6
9,10	89.0	4600	1.0	11,12	3000	1.1

Table 5: Code numbers defined for the FY-3A satellite instruments in IFS.

	Satellite-id	IRAS	MWTS	MWHS	MWRI
IFS/Bufr_code	154/153	963	964	965	966
IFS/ODB	FY3A:520	42	40	41	43
IFS/RTTOV	23	42	40	41	43

Table 6: FY-3A MWTS channel characteristics used for RT coefficients generation

Channel number	Frequency design spec. / GHz	Bandwidth design spec. / MHz	Frequency measured pre-launch / GHz	Bandwidth measured pre-launch / MHz	Frequency tuned post-launch / GHz	Bandwidth tuned post-launch / MHz
1	50.30	180	50.26213	162	50.27213	162
2	53.596	170×2	53.60146	178.1×2	53.59846	178.1×2
3	54.94	400	54.98109	375.8	54.97109	375.8
4	57.29	330	57.33962	316.8	57.15962	330

Table 7: Bias predictors implemented in CY35R2.

p0: 1 (constant)
p1: 1000-300hPa thickness
p2: 200-50hPa thickness
p3: T_skin
p4: total column water
p5: 10-1hPa thickness
p6: 50-5hPa thickness
p6: surface wind speed
p7: nadir viewing angle
p8: nadir view angle^2
p9: nadir view angle^3
p10: nadir view angle^4
p11: cos solar zen angle
p12: solar elevation

Table 8: Used bias predictors in CY35R2, by FY-3 sensor type.

Instrument	Channel number	Number of predictors	Used predictor
MWTS	1	4	p0,p8,p9,p10
MWTS	2,3,4	8	p0,p1,p2,p5,p6,p8,p9,p10
IRAS	1,2,3,16,17,19,20	9	p0,p1,p2,p5,p6,p8,p9,p10,p12
IRAS	4,5,6,7,8,9,15,18	8	p0,p1,p2,p5,p6,p8,p9,p10
MWHS	1,2	4	p0,p8,p9,p10
MWHS	3,4,5	8	p0,p1,p2,p5,p6,p8,p9,p10
MWRI	1-10	7	p0,p3,p4,p7,p8,p9,p10

References

Andersson, E., E. Hólm, P. Bauer, A. Beljaars, G. A. Kelly, A. P. McNally, A. J. Simmons, and J.-N. Thépaut, 2007: Analysis and Forecast Impact of the Main Humidity Observing Systems. *Quarterly Journal of the Royal Meteorological Society*, **133**, 1473–1485.

Bauer, P., A. Geer, P. Lopez, and D. Salmond, 2010: Direct 4D-Var Assimilation of All-sky Radiances. Part I: Implementation. *ECMWF Technical Memoranda Number 618*, ECMWF, Shinfield Park, Reading, UK, ECMWF.

Bell, W. and Coauthors, 2008: The Assimilation of SSMIS Radiances in Numerical Weather Prediction Models. *IEEE Transactions on Geoscience and Remote Sensing*, **46**, 884–900.

Bell, W., S. Di Michele, P. Bauer, T. McNally, S. J. English, N. Atkinson, F. Hilton, and J. Charlton, 2010: The Radiometric Sensitivity Requirements for Satellite Microwave Temperature Sounding Instruments for Numerical Weather Prediction. *Journal of Atmospheric and Oceanic Technology*, **27 (3)**, 443–456.

Bormann, N., 2009: Characterisation and Use of NOAA-19 ATOVS Data. *ECMWF Technical Report*, **0946**.

Challon, G., F. Cayla, and D. Diebel, 2001: IASI: An Advanced Sounder for Operational Meteorology. *Proceedings of the 52nd Congress of IAF*, Toulouse France.

Chevallier, F., S. D. Michele, and A. McNally, 2006: Diverse Profile Datasets from the ECMWF 91-level Short-range Forecasts. *Technical Report, NWPSAF-EC-TR-010*.

Dee, D., 2004: Variational Bias Correction of Radiance Data in the ECMWF System. *Proceedings of the ECMWF workshop on assimilation of high spectral resolution sounders in NWP*, 97–112.

Dong, C., et al., 2009: An Overview of a New Chinese Weather Satellite FY-3A. *Bulletin of the American Meteorological Society*, **90**, 1531–1544.

English, S. J., R. Saunders, B. Candy, M. Forsythe, and A. Collard, 2004: Met Office Satellite Data Observing System Experiments. *3rd WMO Workshop on the Impact of Various Observing Systems in Numerical Weather Prediction*, Alpbach, Austria, WMO.

Geer, A. and P. Bauer, 2010: Enhanced Use of All-sky Microwave Observations Sensitive to Water Vapour, Cloud and Precipitation. *ECMWF Technical Memoranda Number 620*, ECMWF, Shinfield Park, Reading, UK, ECMWF.

Geer, A., P. Bauer, and P. Lopez, 2008: Lessons Learnt from the Operational 1D+4D-Var Assimilation of Rain- and Cloud-affected SSM/I Observations at ECMWF. *Quarterly journal of the Royal Meteorological Society*, **134**, 1513–1525.

Geer, A., P. Bauer, and P. Lopez, 2010: Direct 4D-Var Assimilation of All-sky Radiances. Part II: Assessment. *ECMWF Technical Memoranda Number 619*, ECMWF, Shinfield Park, Reading, UK, ECMWF.

Goodrum, G., K. Kidwell, and W. Winston, 2009: NOAA KLM Users Guide with NOAA-N, -N-Prime Supplement. NOAA. *http://www2.ncdc.noaa.gov/docs/klm/cover.htm*, 488–494.

Hilton, F., N. C. Atkinson, S. J. English, and J. R. Eyre, 2009: Assimilation of IASI at the Met Office and Assessment of Its Impact through Observing System Experiments. *Quarterly journal of the Royal Meteorological Society*, **135**, 495–505.

Kawanishi, T., et al., 2003: The Advanced Microwave Scanning Radiometer for the Earth Observing System (AMSR-E), NASDA's Contribution to the EOS for Global Energy and Water Cycle Studies. *IEEE Transactions on Geoscience and Remote Sensing*, **41**, 184–194.

Kelly, G. A., P. Bauer, A. J. Geer, P. Lopez, and J.-N. Thépaut, 2008: Impact of SSM/I Observations Related to Moisture, Clouds, and Precipitation on Global NWP Forecast Skill. *Monthly Weather Review*, **136 (7)**, 2713–2726.

LeMarshall, J., et al., 2006: Improving Global Analysis and Forecasting with AIRS. *Bulletin of the American Meteorological Society*, **87**, 891–894.

Li, Q., 2001: Development of Chinese Geostationary Meteorological Satellite. *Spacecraft recovery and remote sensing*, **22**, 13–19.

Matricardi, M., F. Chevallier, G. Kelly, and J.-N. Thepaut, 2006: An Improved General Fast Radiative Transfer Model for the Assimilation of Radiance Observations. *Quarterly journal of the Royal Meteorological Society*, **130**, 153–173.

Meng, Z., 2004: The Polar Orbit Meteorological Satellite in China. *Engineering Science*, **6**, 1–5.

Zhang, P., J. Yang, C. Dong, N. Lu, Z. Yang, and J. Shi, 2009: General Introduction on Payloads, Ground Segment and Data Application of Fengyun 3A. *Frontiers of Earth Science in China*, **3**, 367–373.